

# POLITECNICO DI TORINO

Master's Degree in Biomedical Engineering

Master's Degree Thesis

## **Measurements and Data Elaboration with a Microwave Imaging System for Brain Stroke Monitoring**



### **Supervisor**

Prof.ssa Francesca Vipiana

### **Co-Supervisors**

Dr. Jorge Alberto Tobon Vasquez

Ing. David Orlando Rodriguez-Duarte

### **Candidate**

Federica Farinelli

ACADEMIC YEAR 2019/2020



# Contents

<b>Abstract.....</b>	<b>6</b>
<b>1 Introduction.....</b>	<b>10</b>
1.1 Brain Stroke.....	10
1.2 Existing Brain Imaging Techniques.....	13
1.2.1 Computed Tomography.....	13
1.2.2 Magnetic Resonance Imaging.....	15
<b>2 Microwave Imaging.....</b>	<b>17</b>
2.1 Microwaves.....	17
2.2 Dielectric Properties of Brain.....	18
2.3 Inverse Scattering Problem.....	20
<b>3 Materials and Methods.....</b>	<b>23</b>
3.1 MWI Prototype.....	23
3.1.1 Matching Medium and Working Frequency.....	24
3.1.2 Antennas.....	27
3.1.3 Vector Network Analyzer and Switching Matrix.....	29
3.1.4 Head Anthropomorphic Phantom.....	31
3.2 Image Reconstruction Algorithm.....	32
3.3 Experimental Design.....	33
<b>4 Experimental Measurements and Results.....</b>	<b>36</b>
4.1 Small Plastic Ball.....	36

4.2 Balloon Filled with Blood.....	42
4.3 Cylindrical Case Target.....	48
4.4 Calibration Procedure.....	60
4.4.1 External Channel.....	60
4.4.2 Calibration with External Channel.....	63
<b>5 Further Analysis.....</b>	<b>64</b>
5.1 Ictus Monitoring.....	64
5.2 Multifrequency Analysis.....	69
5.3 Check: “False Positive”.....	72
<b>6 Discussion.....</b>	<b>75</b>
<b>7 Conclusion and Future Perspectives.....</b>	<b>77</b>
<b>Bibliography.....</b>	<b>79</b>



# Abstract

Nowadays brain stroke is the second cause of death and the third cause of permanent disabilities worldwide and for this it requires timely diagnosis and treatment in order to reduce the risk of death or further damages for the patient.

In this regard, the most adopted clinical imaging techniques are Computed Tomography and Magnetic Resonance Imaging, but, although they are accurate and with high resolution, they have the drawbacks of being expensive, bulky and not portable, not comfortable for the patient and not suitable for a continuous monitoring, which is essential after a stroke onset.

Moreover, the Computed Tomography uses ionizing radiation as X-Rays, so it is even harmful and not appropriate for repeated examinations.

These evidences have led to the necessity to develop a new diagnostic device based on Microwave Imaging (MWI) technology, which is relatively low cost, not harmful since it uses non-ionizing radiation, not invasive for the patient and above all it can be employed for bedside monitoring and frequent examinations.

Microwave Imaging technology exploits the fact that the stroke has different dielectric properties (relative permittivity and conductivity) respect to brain healthy tissues at microwave frequencies and, hence, evaluating this dielectric contrast, it is possible to obtain an image as the location and shape of brain stroke.

A MWI prototype for brain stroke monitoring has been realized at the Antenna and Electromagnetic Compatibility Laboratory (Politecnico di Torino).

The work of this thesis focuses on the experimental assessment of this MWI prototype through an extensive measurement campaign, reconstructing with different types of targets to simulate the presence of a stroke.

The MWI system is composed by 24 printed monopole antennas, placed conformal to a head phantom, that is filled with a liquid mixture whose dielectric properties are those of an averaged brain tissue at microwave frequencies.

Each antenna, immersed in a brick made of graphite and urethane rubber (which acts as a coupling medium), works as a transmitter to illuminate the phantom and as a receiver to collect the field scattered by the head.

This is made possible thanks to a  $2 \times 24$  switching matrix and to a Vector Network Analyzer which measures the  $24 \times 24$  scattering matrix useful for the image reconstruction; all the components are controlled via laptop.

The image is then obtained through a differential approach: the difference between two scattering matrices related to two different time instant (one with a target-stroke inside the phantom and one without it) is given in input to an image reconstruction algorithm based on the Born approximation and the TSVD truncated singular value decomposition, so that the inverse scattering problem is solved and the dielectric contrast reconstructed.

The first measurements have been made with a small plastic ball with a precise geometry and easier to locate in the liquid inside the phantom: although some inaccuracies (especially in matching the right position), the system shows the ability to image the object.

The next acquisitions instead have been made with a target whose dielectric properties are the same of the blood so that it could simulate a hemorrhagic stroke; an immediate but basic case is a balloon filled with a liquid, which mimics the blood, inserted in the phantom through sticks, while a more refined target has been obtained taking an almost cylindrical case filled with blood mimicking liquid and put also in different positions of the head.

The images obtained with the cylindrical-case target are less noisy than the ones with the balloon and also the target is more realistic and easier to manage; the results show that also in these cases, the device is able to see the object inside the brain, even if it makes more difficulty in catching and so reconstructing the right position of the target.

The current limits reside however in the spatial resolution and in a quite high sensitivity to various perturbations, such as temperature or measurement noise.

During the thesis, moreover, calibration procedures have been investigated, placing two of the 24 antennas external to the phantom and considering them as reference channel, in order to understand if their signal, not dependent on the target, can help to correct the measurements.

The next possible steps to improve this MWI prototype regards the measurements with smaller targets to check if the system can image them and measurements with a target which simulates also an ischemic stroke, that could be also mimicked with a proper mix of liquids as the other liquid.

Furthermore, there is interest in creating a “stroke monitoring”, for example acquiring measures rotating the target from a vertical position to a horizontal one.

All these tests have as the final challenge the realization of a portable 3-D wearable MWI helmet.



# 1 Introduction

## 1.1 Brain Stroke

A stroke is a medical pathology which affects the arteries and it occurs when the blood flow is stopped leading to cells death in few minutes.

Brain stroke, in particular, is a cerebrovascular disease which happens when a blood vessel within the brain area is blocked and it cannot carry oxygen and nutrients to neurons anymore.

Blood flow interruption can be caused either by a clot or by a rupture in the vessel and both cases bring the brain region interested by the stroke not to working properly; the stroke determines, in fact, long-term disabilities, lasting brain damages or even death [1].

Stroke is in general divided into two types:

- the ischemic stroke, caused by a clot which obstructs the blood flow in the artery often due to fatty deposits in the vessel
- the hemorrhagic stroke, caused by a weakened vessel which bursts and bleeds in the surrounding brain area compressing brain tissues [2].

The ischemic one represents the most common stroke in the world (about the 87%) while the hemorrhagic one is the less common (13%) but the deadliest.

Signs and symptoms of the disease usually include inability to move parts of the body, difficulty speaking, vision problems, loss of balance or coordination and also severe headache for the hemorrhagic stroke, but they appear after the stroke has occurred.

Each year nearly 795 000 people have a stroke and precisely 610 000 of these experiences a first attack, while 185 000 people have not a new stroke but a recurrent attack.

The major risk factors inducing stroke can be listed as follows [3]:

- high blood pressure

- diabetes
- heart disease (atrial fibrillation, coronary heart disease, heart valve disease)
- high blood cholesterol
- smoking
- previous attack
- genetics
- age
- sex
- race and ethnicity.

The figure 1 shows the high incidence of this pathology all around the world, depending on age, sex and country.

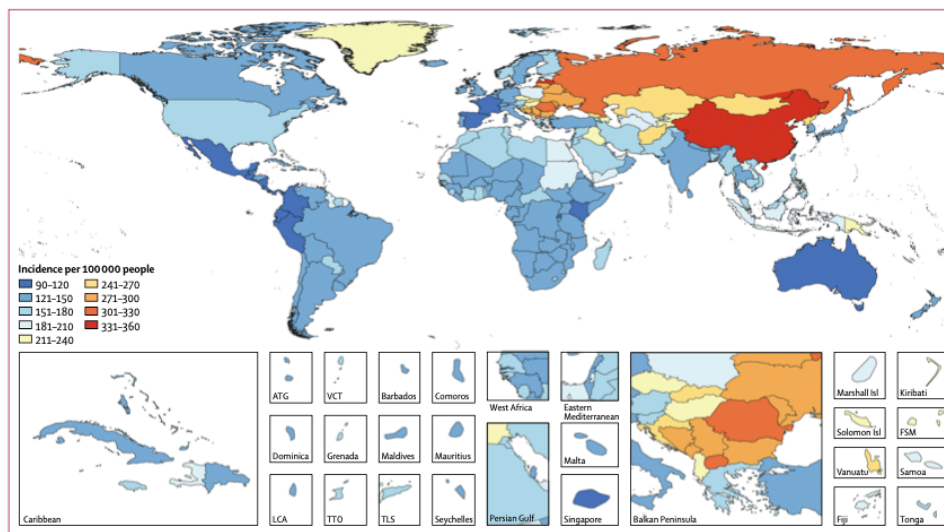


Figure 1. Age-standardized stroke incidence, 2016 [4]

Since brain stroke is recognized as the second most common cause of death worldwide and the third most common cause of disability [5], it represents a critical medical issue and it needs timely diagnosis and treatment in order to reduce the risk of death, further disabilities or damages for the patients and even a second onset. The diagnostic exams done by clinicians to detect the presence of a stroke are normally neurological examinations supported by medical imaging, which enable to recognize the type and the location of the brain affected area, often accompanied by other tests to underline the cause of the onset, like electrocardiogram and blood tests.

## 1.2 Existing Brain Imaging Techniques

As anticipated, neuroimaging is essential to diagnose the presence of a stroke and it should be done for all patients suspected to having an attack, since it permits to distinguish between ischemia and hemorrhage and to exclude stroke mimics such as tumor. Nowadays, the most used and assessed imaging techniques in order to evaluate brain lesions are above all the Computed Tomography (CT) and the Magnetic Resonance Imaging (MRI) [6].

### 1.2.1 Computed Tomography

Computed Tomography reproduces a 3-D image section of an internal part of the body through a series of projections of the object irradiated by X-Rays.

The object of interest exposed to X-Rays, in fact, absorbs these radiations according to the Lambert-Beer's law

$$I(x) = I_0 e^{-\mu x} \quad (1)$$

where:

- $I_0$  is the initial X-Rays intensity which illuminates the object
- $\mu$  is the attenuation coefficient typical of each biological tissue
- $x$  is the path traveled by the rays across the object
- $I$  is the final intensity of X-Rays beam, which is attenuated during the propagation in the object.

By measuring this attenuation, a slice so a 2-D projection of the part of the body is reproduced; the 3-D image of the anatomical part is then obtained by acquiring many

projections of the same object irradiated from different angles in order to reconstruct the entire volume [7].



Figure 2. An example of CT device [7]

CT is normally the first scan to which the patient is subjected and it is more sensitive to detect intracranial hemorrhage; this imaging modality, in fact, is used to discriminate hemorrhagic stroke from ischemic one even up to five days after the onset, since it appears with higher density respect to the ischemic stroke, so the whiter brain area is visible respect to the darkest one associated to the ischemia [8].

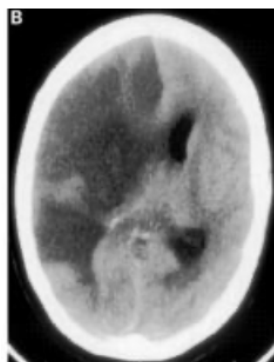


Figure 3. A CT image of ischemic stroke [8]

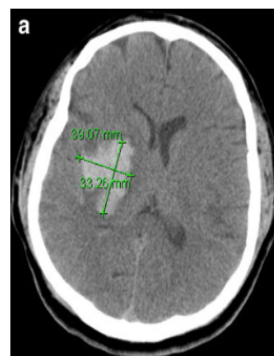


Figure 4. A CT image of hemorrhagic stroke [6]

## 1.2.2 Magnetic Resonance Imaging

The Magnetic Resonance Imaging (MRI) is another diagnostic technique which permits to obtain 3-D images of internal parts of the human body, particularly efficient with soft tissue including the brain.

It is based on the interaction between the hydrogen protons present in the matter (so in the biological tissues too) and two magnetic fields: firstly a constant field is applied in order to create a magnetization vector, which is the result of the sum of all the magnetic moments related to each protons excited by the field; secondly a radiofrequency magnetic field is applied to perturb the magnetization vector. The image is then got measuring the “relaxation time” necessary to restore the equilibrium condition in the examined object, after the radiofrequency field is stopped; the evolution in time of the components of the magnetization vector is the signal useful to collect the 3-D image [9].



*Figure 5. An example of MRI device [9]*

MRI exam is effective especially to detect ischemic stroke more than CT, also in young patients who are suspected to have a stroke even more difficult to be

diagnosed; moreover with the right sequence of excitation, MRI can recognize hemorrhage too in particular within the first six hours after the onset [8].



*Figure 6. An example of MRI of acute ischemia [11]*

Although CT and MRI are the most adopted and reliable diagnostic technologies and in spite of their high resolution, they have several drawbacks which limit the use of these two devices in the detection of the stroke.

Both the instruments are expensive especially for MRI, time-consuming (the acquisition requires more or less dozens of minutes and a real time image is not possible), not portable and bulky (because of their size), available only in the hospital; considering their structure, moreover, they can induce claustrophobia in patients who suffer of staying in small and closed environments and MRI is also noisy, while the CT has the important concern of working with ionizing radiation as X-Rays, which are harmful for the health.

For these reasons, the two techniques cannot be used so frequently for repeated examinations and above all they are not suitable for a continuous monitoring, fundamental to take the patient under control after the attack [12].

All these considerations have led to the necessity of having a new imaging technology which is able to do a continuous monitoring not only in the hospital but even a bedside monitoring and a timely diagnosis right away in ambulance, as complementary to the existing and assessed technologies.

This is the starting point for a Microwave Imaging System.

# 2 Microwave Imaging

## 2.1 Microwaves

Microwaves are non-ionizing electromagnetic radiation included in the frequency range between 300MHz and 300GHz.

Since they are not harmful, they can be used for imaging in medical applications.

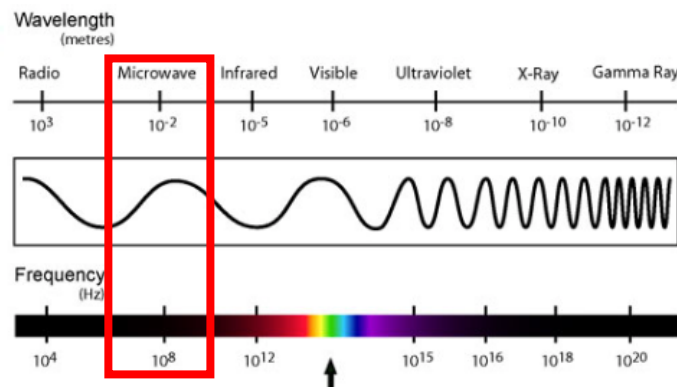


Figure 7. Electromagnetic spectrum [1]

This new technique is very attractive currently as a diagnostic tool especially for brain stroke, because it can offer several advantages:

- safety for the patient
- easier exams both for patients and clinicians
- not-invasive and not-contacting methodology
- relatively low cost
- penetration even in materials opaque to the light
- possibility to repeat the exam and to have monitoring [13] and [14].

There are also some disadvantages, discussed during the thesis, while in the following paragraph the basic principles of Microwave Imaging (MWI) are explained.

## 2.2 Dielectric Properties of Brain

The interaction between an electromagnetic field and an object depends on the dielectric properties of the object taken into account and they determine the transmission, the reflection or the absorption of the electromagnetic wave along the material in different ratios.

The same happens when a radiation interacts with the human body, because the different propagation of the EM waves along biological tissues is due to their dielectric properties, which are the relative permittivity and the conductivity and which change with the frequency.

The permittivity represents the ability of the tissue to store energy when it is exposed to an electromagnetic field, while the conductivity represents the dissipation of the tissue, since it absorbs part of the energy and converts it partially into heat [15].

As regard particularly the brain when exposed to a microwave field, its dielectric properties can be synthesized with the figures 8 and 9, according to the mathematical Cole-Cole model [16]:

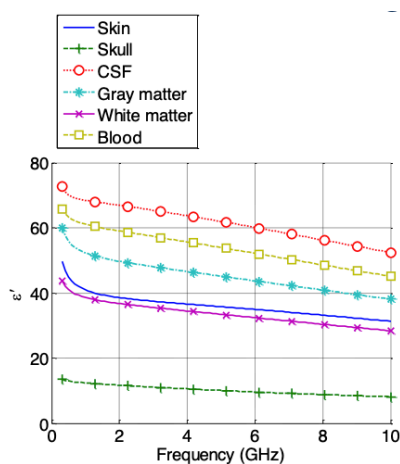


Figure 8. Relative permittivity [14]

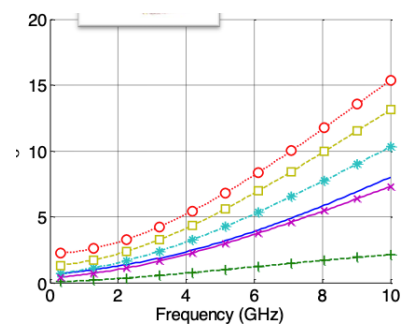


Figure 9. Conductivity [14]

It is possible to notice that the two properties change with the increasing of the frequency and precisely the relative permittivity tends to decrease, while the conductivity grows, leading also to an increasing of the losses in the tissues.

This means that the microwave is attenuated during its propagation in the biological tissue; it is important, in fact, to choose a properly working frequency to assure a good penetration depth.

The basis of MWI resides right in the fact that healthy brain tissues have different value of dielectric properties respect to the injured area; diseases like stroke can change the properties of the tissues and for this MWI exploits dielectric contrast between the stroke and the rest of the healthy brain to reconstruct the image [17].

In order to evaluate this dielectric contrast, Microwave Imaging Technology has to solve the so-called inverse scattering problem.

## 2.3 Inverse Scattering Problem

The scattering phenomenon occurs when an electromagnetic radiation, interacting with the matter, undergoes a deviation of trajectory; the same happens when a microwave incident field illuminates an object, called scatterer, and the perturbed field generated by the presence of the scatterer is defined scattered field.

The objective is to determine the properties of the scatterer, like permittivity, shape and position, knowing the incident field and measuring the scattered field: this is the inverse scattering problem.

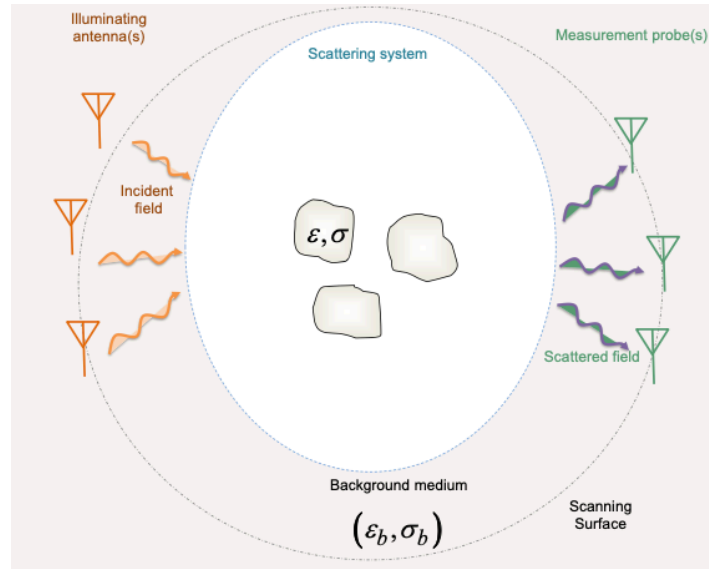


Figure 10. A scheme of scattering system [18]

In MWI technology, the scatterer is represented by the stroke and this imaging methodology solves the inverse scattering problem to obtain the dielectric contrast in brain tissues, which can be defined as [19]:

$$\chi = \frac{\varepsilon(r) - \varepsilon_b}{\varepsilon_b} \quad (2)$$

where  $\varepsilon(r)$  is the permittivity of the scatterer so of the stroke and  $\varepsilon_b$  is the permittivity of the background medium (that is the brain).

The problem is, however, ill-posed and the dependence of the scattered field on the contrast function is nonlinear

$$E^S = L(\chi) \quad (3)$$

since the  $L$  operator, which relates the measured scattered field ( $E^S$ ) and the unknown dielectric contrast, is nonlinear.

An approach to solve the inverse problem is the linearization through Born approximation, which is applied when the scattering is weak and the total field inside the scatterer can be approximate with only the incident field [20]; the formula (3), hence, becomes

$$E^S = L_{Born}(\chi) \quad (4)$$

where  $L_{Born}$  is now linear.

To invert the equation (4) and calculate the contrast, instead, a reliable method is the TSVD Truncated Singular Value Decomposition, which factorizes the scattering operator  $L_{Born}$  into the product of three matrices, in the following way

$$\chi = \sum_{n=1}^N \frac{1}{\sigma_n} \langle E^S, [un] \rangle [vn] \quad (5)$$

where  $v_n$  and  $u_n$  are respectively the left and the right singular vectors, while  $\sigma_n$  are the singular values and  $N$  the truncated index [18].

These are the basis of an image inverse algorithm which reproduces the diagnostic image.

Therefore, the design of a MWI system can be schematized in the following way by the figure 11:

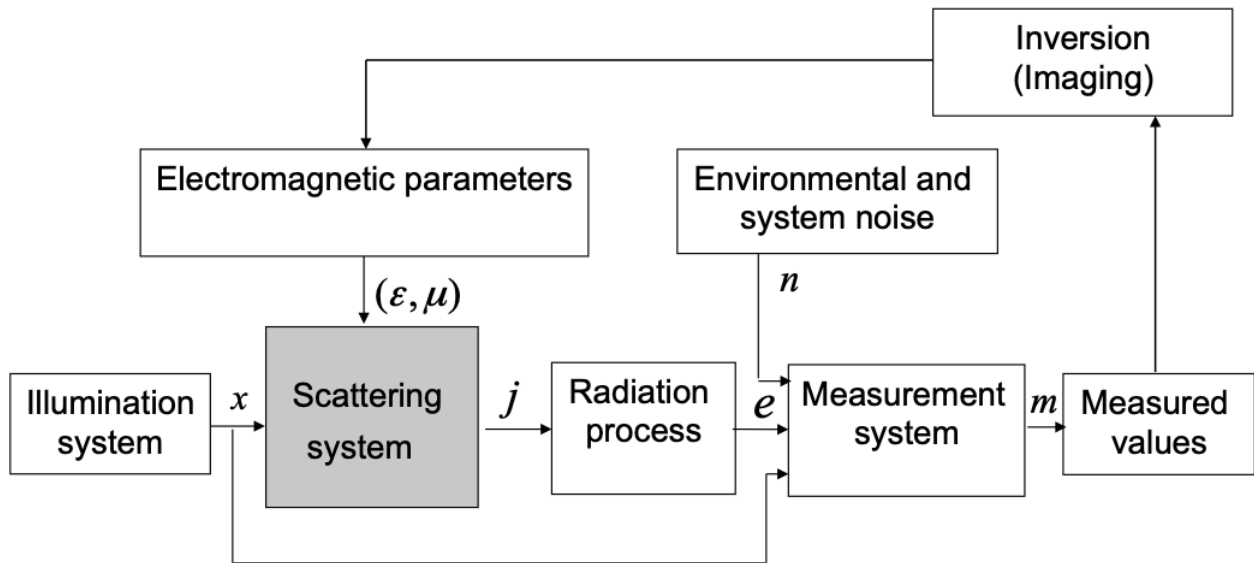


Figure 11. Scheme of MWI medical device [13]

in which  $x$  can be the incident field, while  $e$  the scattered one.

# 3 Materials and Methods

A prototype of low-complexity Microwave Imaging technology has been realized in the Antenna and Electromagnetic Compatibility Laboratory of Politecnico di Torino and it is the one employed during the thesis.

In this chapter the description of the 3-D MWI device is presented with its constituent components, the working of the image algorithm and the types of experimental measurements done.

## 3.1 MWI Prototype

The system is essentially based on the measure of the scattering parameters of the body under test, which is the stroke simulated with a target, through antennas, which radiate a linearly polarized microwave field and then collect the signals obtained after the interaction of the microwave with the target.

These parameters are, hence, given in input to the image reconstruction algorithm.



*Figure 12. Overview of MWI system at LACE. From left to right: VNA, bench power supply, switching matrix, antennas and head phantom connected through coaxial cables, box with reference antennas*

### 3.1.1 Matching Medium and Working Frequency

The first step to realize a MWI device is setting the proper working frequency, with which irradiate the tissues under exam, and the choice of a good coupling medium to put between the tissues and the MWI probes, which are the antennas, in order to improve the coupling between them and to acquire a better signal, which otherwise would be too exiguous.

Two criteria, to take into account to choose these two design parameters, are:

- the maximization of the incident microwave power, which has to penetrate the brain tissues and which is influenced by electrical discontinuity;
- the highest possible spatial resolution in order to be able to detect even small variations and which is determined by the wavelength of the matching medium [21].

A planar model of the head is adopted to assess the choice of the type of medium and of the working frequency; it consists of five layers representing the brain tissues, each of them characterized by their dielectric properties, which are in order the skin, the fat, the cortex bone, the cerebrospinal fluid and the inner one is the brain, considered as an average of grey and white matter.

A scheme of this model is shown by the figure 13

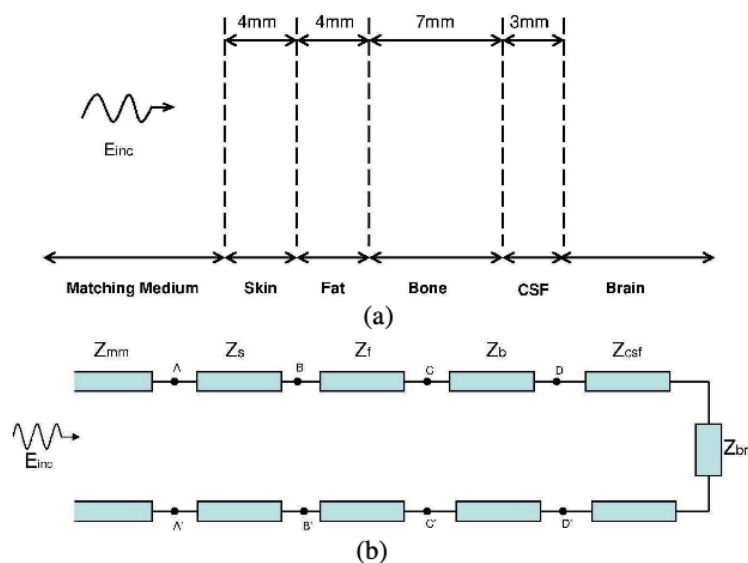


Figure 13. Planar layer model of human head [21]

where  $Z_n$  stands for the impedance of the tissue defined as

$$Z_n = \sqrt{\frac{\mu_0}{\varepsilon_0 \varepsilon_n}} \quad (6)$$

and  $\varepsilon_n$  is complex permittivity of the corresponding medium,  $\varepsilon_0$  and  $\mu_0$  the electric permittivity and the magnetic permeability in the vacuum.

To analyze the incident power penetrating the brain, the Transmission Line formalism is adopted and the transmission coefficient is calculated as

$$T = 1 - \Gamma \quad (7)$$

where  $\Gamma$  is the reflection coefficient at the section AA', which is the interface between the matching medium and the first layer, that is the skin, defined as

$$\Gamma = Z_{AA'} - Z_{mm} / Z_{AA'} + Z_{mm} . \quad (8)$$

The transmission coefficient at (7) is calculated for a frequency range of [100MHz-10GHz] and for a coupling medium whose relative permittivity varies from 1 to 80.

Firstly, a lossless medium is considered and three bands of frequency are identified:

- a “forbidden band” between 1.5GHz and 4GHz, where the  $T$  is too low and not appropriate for brain imaging;
- a higher band with frequencies upper than 4GHz, which is not convenient since the penetration depth is scarce for the brain tissues;
- a lower band with frequencies lower than 600MHz, which offers a quite good penetration but only for medium with  $\varepsilon_r=20$  and moreover it is not suitable for a sufficient spatial resolution.

Secondly, the transmission coefficient is computed for a lossy medium, considering a varying conductivity and taking fixed the permittivity; the results show that the conductivity does not influence the  $T$  value (7) and that the convenient frequency range is [0.6GHz-1.5GHz] [22].

All these considerations lead to the final choice of a coupling medium with  $\epsilon_r=20$  and a working frequency around 1GHz, to guarantee the best compromise between penetration and resolution, also reducing the losses.

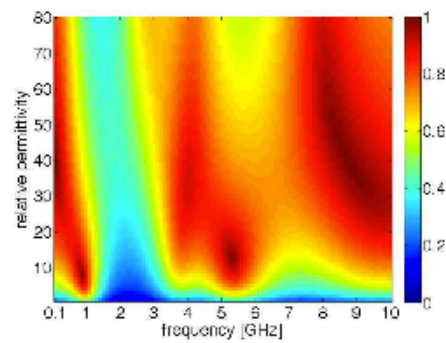


Figure 14. Transmission coefficient in function of the frequency and the relative permittivity of a lossless matching medium of [22]

### 3.1.2 Antennas

The antennas are the microwave probes used to irradiate the object under test and then to receive the signal scattered by the object.

The antennas employed in the system are monopole printed antennas on a FR4 dielectric substrate, which are placed conformal to a 3-D phantom representing the human head [23].

The figure 14 shows the realized antennas

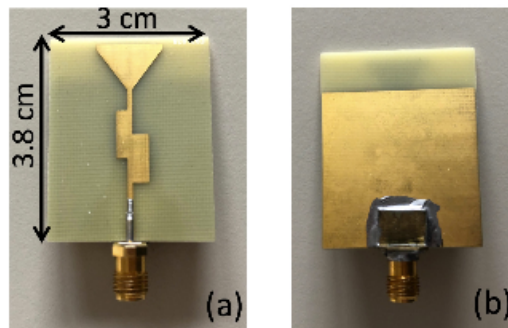


Figure 15. Monopole printed antenna: top (a) and bottom (b) [23]

where the top is the transmission line, while the bottom is the ground plane.

Each antenna is immersed in a brick made of urethane rubber-graphite which works as a coupling medium and whose relative permittivity is around 20; using this solid rubber enables to place the antennas conformally around the head.



Figure 16. Brick antenna [24]

The number and the position of the antennas are determined considering the discretization errors, due to the fact that the scanning is not continuous, but made with an array of a finite number of antennas.

The good compromise to obtain a sufficient resolution and a low-complexity system is given by a set of 24 antennas [25].

### 3.1.3 Vector Network Analyzer and Switching Matrix

The Vector Network Analyzer (VNA) measures the Scattering parameters and describes the relation between the ports of an electrical device.

For a 2-ports device, such as in the case of the antennas of this prototype, the input-output signals are so related as in figure 16:

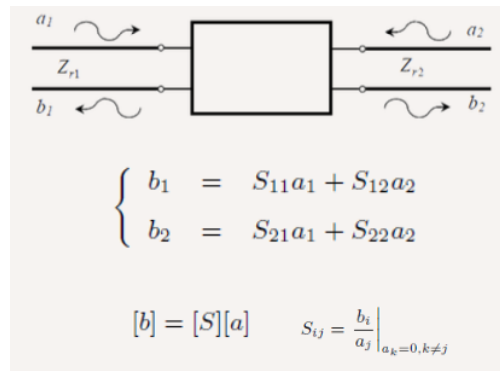


Figure 17. 2-ports device representation [24]

where  $a_k=0$  is obtained when the transmission line terminates with an impedance equal to  $Z_{rk}$ .

The scattering matrix, hence, contains the reflection coefficients to port1 along the main diagonal, while the transmission coefficients from port1 to port2 out of the main diagonal.

In this application, due to reciprocity (passive and nonmagnetic objects), the S-matrix is symmetrical.

The VNA used [26], generates the incident signals, also thanks to a bench power supply set to 24V, and received them, computing the scattering parameters of the system.

To enable each antenna to work both as transmitter, to illuminate the phantom, and as a receiver to collect the scattered signals, a 2x24 switching matrix is also used, connected to the two ports of the VNA through flexible coaxial cables.

The switching matrix, in fact, can change the antenna which is transmitting or receiving so that while one of the antennas is transmitting, the other 23 ones are receiving in turn.

At the end of a measurement, each antenna has transmitted and received the signals and in this way the Scattering matrix of the system is measured, which is the input data for the image reconstruction algorithm [25].

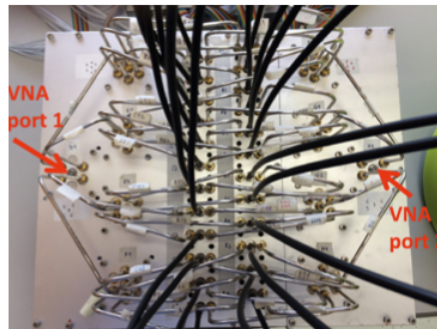


Figure 18. 2X24 Switching matrix [23]

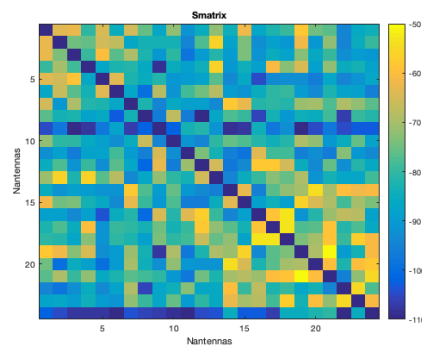


Figure 19. An example of scattering matrix (the self-terms in general forced to zero to underline the transmission ones): the intensity of the scattering parameters is expressed in dB

Moreover, the Ethernet connectivity is exploited to use the network so that all these components can be controlled via laptop; even the electromechanical switches are managed with the computer through a MATLAB script.

### 3.1.4 Head Anthropomorphic Phantom

A 3-D anthropomorphic phantom is used to reproduce the human head, which has to be illuminated with microwaves through the arrays of antennas.

The phantom is realized in Acrylonitrile Butadiene Styrene (ABS) [26], which is a thermoplastic polymer, thanks to the additive manufacturing technique using a Stereolithography file obtained from a MRI image.



Figure 20. Head Phantom [25]

The phantom consists of a cavity, whose maximum section is almost an ellipse with the minor and the major axes respectively of 20 cm and 26 cm.

This cavity is filled with a liquid mixture which mimics the dielectric properties of an averaged human brain tissues; the liquid is made of Triton X-100 (a surfactant), water and salt and its properties are almost  $\epsilon_r=42$  and  $\sigma=0.75$  S/m.



Figure 21. Head phantom filled with "brain" surrounded by brick antennas

## 3.2 Image Reconstruction Algorithm

The image algorithm reconstructs a 3-D image with the location and the shape of the suspected stroke inside the head through the measured scattering matrix.

As already said in the second chapter, the algorithm solves the inverse scattering problem obtaining the unknown contrast function.

Since the goal of MWI system is to monitor the evolution of the stroke during the time after its onset, a differential approach is adopted, in order to reconstruct the variation of the dielectric contrast in brain tissues during the time, which is mapped in the image [27].

For this reason, the input data of the algorithm is a differential scattering matrix, denoted as  $\Delta S$ , which represents the difference between two scattering matrices of the system, measured in two different time instants; the output of the algorithm, instead, is the differential dielectric contrast  $\Delta\chi$ , associated to  $\Delta S$ .

This differential contrast is defined as  $\Delta\varepsilon/\varepsilon_b$ , where  $\Delta\varepsilon$  is the permittivity variation between the two time instants and  $\varepsilon_b$  is the permittivity of the background, that is the reference scenario so the brain at first diagnosis.

Assuming that the differential contrast is a small and localized variation, the Born approximation (4) can be exploited to relate the differential scattering matrix with the differential dielectric contrast, according to the equation

$$\Delta S(r_p, r_q) = L(\Delta\chi) \quad (9)$$

in which  $S$  is the linear operator whose kernel is  $-j\omega\varepsilon_b/4 E_b(r_m, r_p) \cdot E_b(r_m, r_q)$ ,  $E_b$  is the electric field radiated by the antennas in the image domain at the reference state,  $r_m$  the position of the points in which the image domain is discretized,  $r_p$  and  $r_q$  the position of the transmitting and receiving antennas [28].

The contrast is then obtained inverting the equation through the Truncated Singular Value Decomposition (TSVD), factorizing the scattering operator  $L_{Born}$  into the product of three matrices, as follows:

$$\Delta\chi = \sum_{n=1}^{L_t} \frac{1}{\sigma_n} \langle \Delta S, u_n \rangle v_n, \quad (10)$$

where  $u_n, \sigma_n, v_n$  are the singular values of the discretized operator  $S$ , while  $L_t$  is the truncation index, that is a threshold chosen in order to have a compromise between stability and accuracy in the reconstruction, theoretically traceable where there is the change in the slope of Singular Values curve, but in practice the value is lightly lower than the one corresponding to the change of the slope [27].

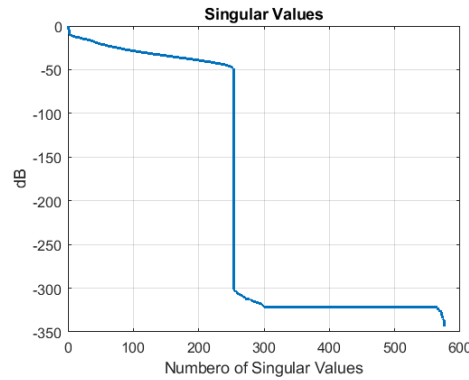


Figure 22- Example of singular value spectrum

Moreover, the realized MWI prototype has been accompanied by a digital twin in order to simulate the behavior of the proposed technology; the simulation is realized thanks to CAD and electromagnetic simulation softwares.

The two main intents of this simulator are to compute the  $E_b$  field used for the kernel of the TSVD operator and to foresee the expected outcomes of the experimental measurements [25].

### 3.3 Experimental Design

The work of this thesis focuses on the experimental validation of the MWI prototype realized at the LACE, through an extensive measurements campaign, in which the capability of the device to image a stroke inside the head is investigated.

All the acquisitions have been made with the system previously described: for each measurement, which spends almost 16 minutes (in this regard some optimizations could be done to make the time shorter), the 24x24 scattering matrix is generated and precisely a 24x24x5 scattering matrix: a multifrequency acquisition is done, so the working frequency is set with a range of five points of frequency ([0.5 1.125 1.75 2.375 3] GHz) and, hence, five scattering matrices are collected for each measurement.

For the reconstruction is then used the matrix that belongs to the selected band, so the second matrix related to 1.125GHz is employed.

Moreover, in the measured scattering matrix, the main diagonal is forced to zero, since the transmission coefficients are the ones used for the image and not the reflection ones, while the rows and the columns related to the antennas 8 and 10 are also put to zero, because these two antennas are removed and placed external to the phantom.

They are put in a box, fixed near the phantom, and they are used as a reference channel, in order to investigate calibration procedure, since in this way their signal do not depend on the target and can be analyzed to see if it can help to improve the measurement results.



*Figure 23. Box with reference antennas. Average head mimicking liquid will be located in the middle to make it similar to the measured scenario.*

To generate the image, hence, a differential scattering matrix is given in input to the algorithm, in particular, two matrices related to two different measurements are used: one with a target inside the phantom in a certain time instant, the other without the target in another time instant; in this way it is possible to analyze if the device is able to reconstruct the object present inside phantom.

The algorithm reorders the two scattering matrices and calculates their difference (between  $S$  with target and  $S$  without it that is the empty measurement assumed as reference); then it computes the TSVD and, by inversion (10), obtains the contrast, which is plotted in different ways.

The types of images with which are presented the results are precisely:

- a 3-D head isometric view so a 3-D rendering of the imaged target, normalizing the differential contrast
- head views in the three main anatomical planes (sagittal y-z axes, frontal x-z axes, coronal x-y axes)
- a energy map, whose intensity is expressed in dB, which is a horizontal cross-section of the 3-D image, taken at a level of the  $z$  axe which better enables the visualization of the reconstructed target.

The experimental assessment is conducted acquiring and elaborating several measurements with three types of target inserted inside the phantom filled with the brain liquid; the realization of the targets and the results obtained are illustrated in the following chapter, which reports the experimental set-up together with the images reconstructed for each of the three targets tested.

# 4 Experimental Measurements and Results

This chapter illustrates the most significant results of the several measurements made with the MWI prototype in different configurations; firstly the experimental set-up is described and then the images obtained are shown.

The acquisitions together with their results are differentiated in three groups according to the target used.

## 4.1 Small Plastic Ball

The first adopted target is a small plastic ball, precisely a sphere of almost 1.25 cm of radius and a relative permittivity around 2.1.

It is fixed to a wooden skewer through a fishing line long nearly 15 cm and it is inserted in the head phantom, full of liquid mimicking the brain, placing the skewer horizontally on the top cavity of the phantom.

The sphere is also enclosed in a piece of latex glove so that it is possible to attach it to the fishing line.



*Figure 24. Plastic ball target*

This kind of target is simple to realize and easy to insert in the phantom; in fact, it does not float in the liquid and the measurements are acquired placing the sphere in different locations of the phantom.

In the three cases reported, the sphere is located at half phantom height (between the top of the head and the eyes) but each of them in different positions; the time passed between the acquisitions (the one with the target and the one without it) is also reported, considering the time instant when the first of the two measurements starts and the time instant when the second of the two ones ends.

Different thresholds for the truncation of the SVD are tested, in particular between -20 dB and -30 dB, and the best visualizations are shown as an image result.

### CASE 1

- target position: lateral central, frontal central, top central
- time passed 50 minutes



Figure 25. Experimental set-up

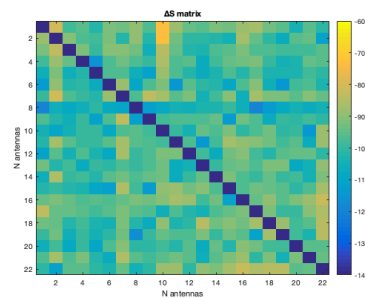


Figure 26. AS matrix

## RECONSTRUCTION

The red circlet in the reconstructed image shows where the target is expected to be seen: all the axes are calibrated in millimeters

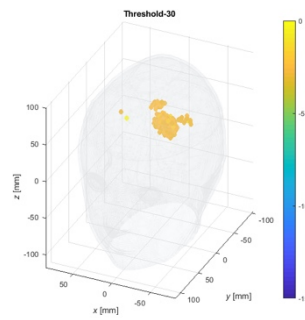


Figure 27. 3-D rendering

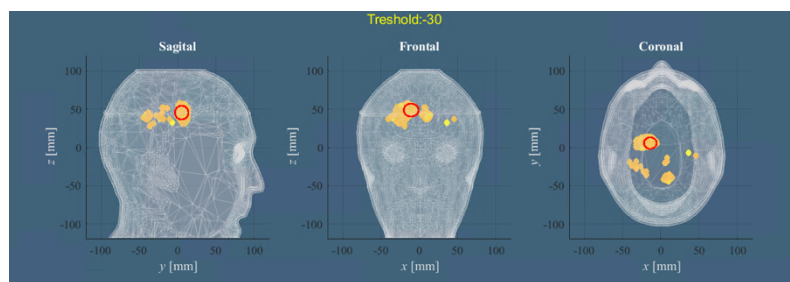


Figure 28. Three main planes views

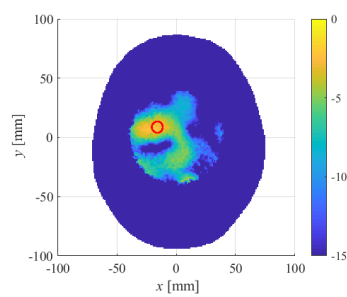


Figure 29. Energy map

## CASE 2

- target position: lateral central-back, frontal central, top central-back
- time passed 56 minutes

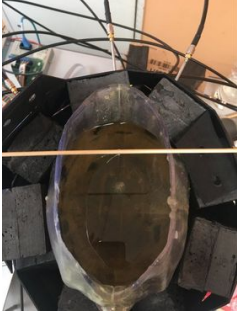


Figure 30. Experimental set-up

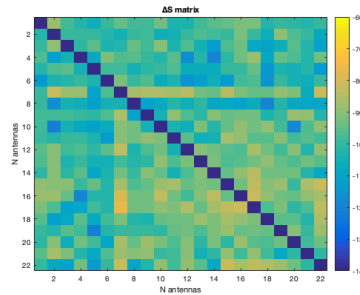


Figure 31.  $\Delta S$  matrix

## RECONSTRUCCION

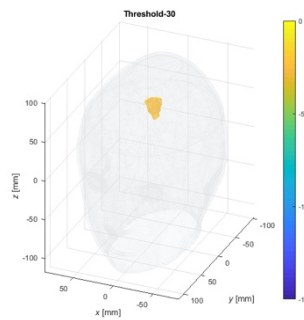


Figure 32. 3-D rendering

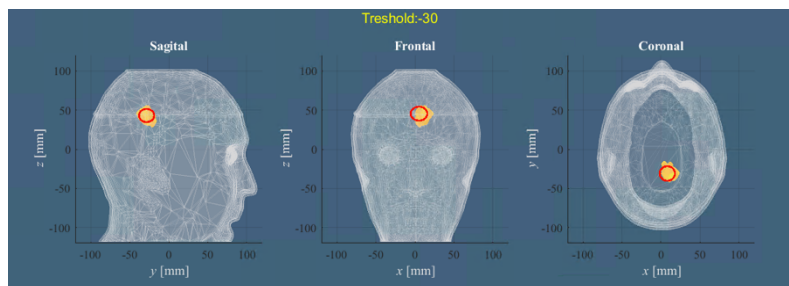


Figure 33. Three main planes views

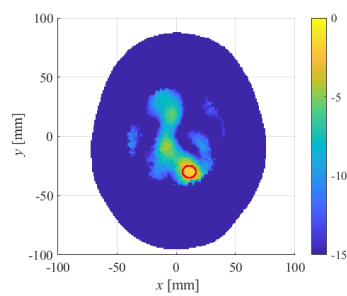


Figure 34. Energy map

### CASE 3

- target position: lateral central-forward, frontal central, top central-forward
- time passed 49 minutes

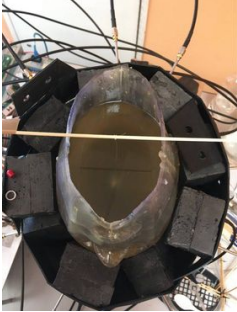


Figure 35. Experimental set-up

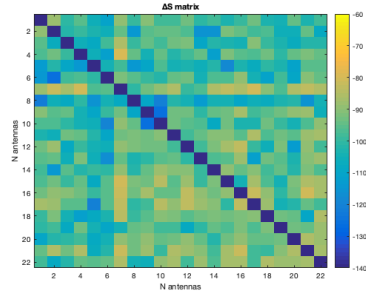


Figure 36.  $\Delta S$  matrix

### RECONSTRUCTION

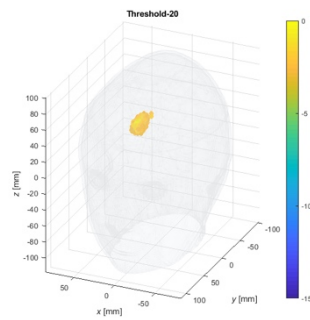


Figure 37. 3-D rendering

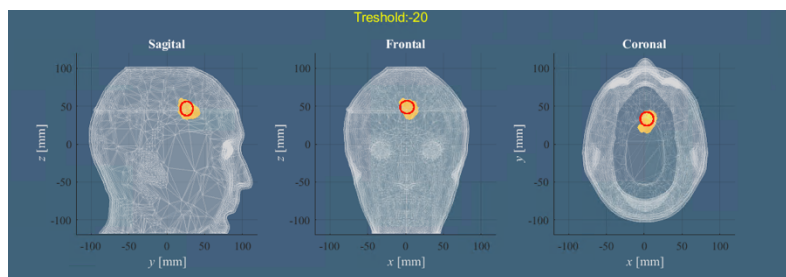


Figure 38. Three main planes views

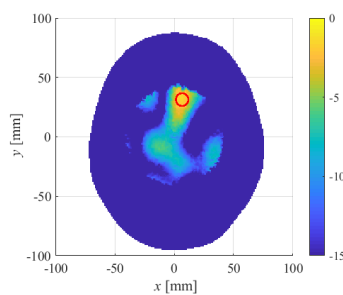


Figure 39. Energy map

The images obtained prove that the MWI prototype is able to image an object; the yellow circle, in fact, represents the target and it is clearly visible, even if its exact position and shape are not always reconstructed precisely (as in case1).

The goal of the plastic ball is, hence, not to mimic a stroke, since its relative permittivity is different respect the one of the blood, but to create a dielectric contrast, which is close to the one of a hemorrhage but with opposite sign [25], so that the system can detect it.

Even if with some inaccuracies between the actual position of the target and the expected one, which can be due to the measurement noise or to liquid mixing when inserting the target, the prototype can see the target and also its reconstruction changes in position with the changing of the position of the target in the experimental set-up.

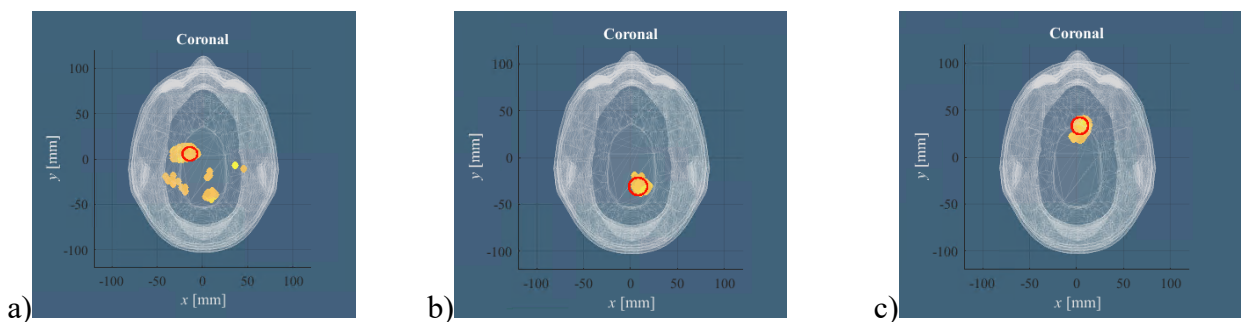


Figure 40. Positions comparison: a) case1 central, b) case2 back, c) case3 forward

The next step is to acquire measurements, using a target with the same dielectric properties of blood in order to really recreate the conditions of a stroke.

## 4.2 Balloon filled with blood

The second two targets used for the measurements campaign want to simulate a hemorrhagic stroke, so they are made in a way for which they can be filled with a liquid whose dielectric properties are the same of blood at microwaves.

The first model of target is simple and immediate to realize: it is made with a balloon, precisely a finger of a latex glove, filled with a liquid that acts as blood, composed of 38% of Triton X-100 and 9.4 g/L of salt whose  $\epsilon_r$  is 61 and  $\sigma$  is 1.6 S/m at 1GHz, then tied to a wooden stick in order to insert it in the phantom [26].

It is quite big, almost 7 cm long and 3 cm large, so that the device is more likely to see it.



*Figure 41. Balloon with blood mimicking liquid as a target*

Other sticks are added at the top of the one linked to the balloon so that the target can be positioned in the phantom, leaning on its cavity; this structure enables also to have a greater stability avoiding the rotation of the stick with the balloon.

The complete target is shown in the photo 41.

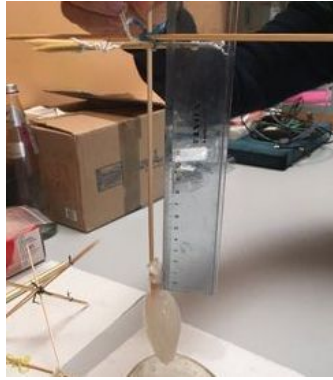


Figure 42. Balloon target

In this set-up, the stick is nearly 16 cm long so the target can reach a depth of 16 cm inside the head phantom, starting from its upper cavity; shifting higher the horizontal sticks, instead, it is possible to make the vertical one longer so that the balloon can reach a depth around 20 cm and in this way the target can be placed in different position or in different height too.



Figure 43. Longer stick



Figure 44. Shorter stick

As for the previous target, the image reconstructions are obtained testing different TSVD threshold, between -20 dB and -30 dB, and the results are shown in the following.

## CASE 1

- target position: lateral central, frontal central, top central slightly to the left
- time passed 56 minutes



Figure 45. Experimental set-up

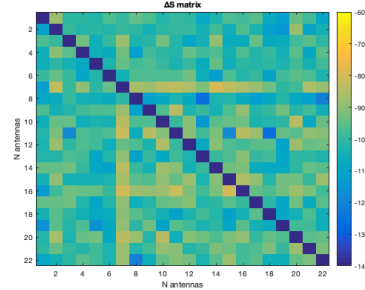


Figure 46.  $\Delta S$  matrix

## RECONSTRUCTION

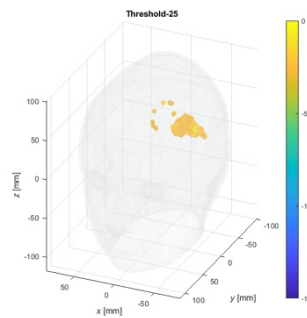


Figure 47. 3-D rendering

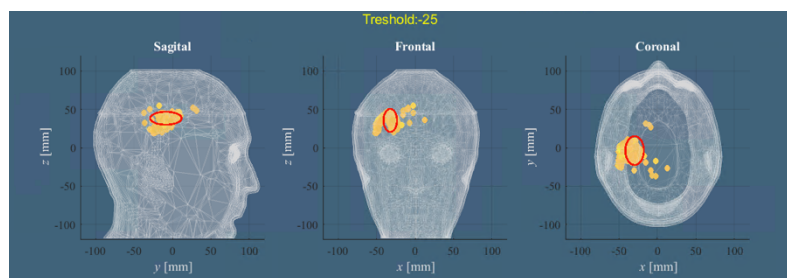


Figure 48. Three main planes views

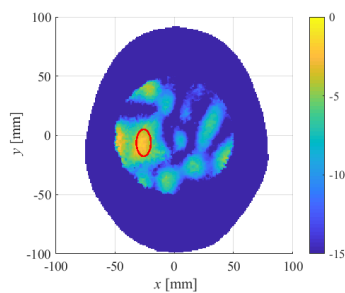


Figure 49. Energy map

## CASE 2

- the same experimental set-up is reconstructed using another reference empty, which is more distant in time
- time passed 1 hour and 56 minutes

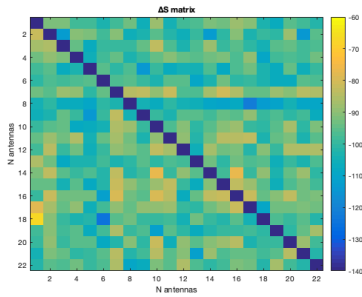


Figure 50.  $\Delta S$  matrix

## RECONSTRUCTION

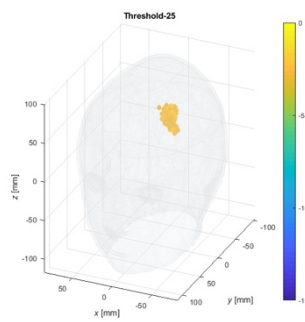


Figure 51. 3-D rendering

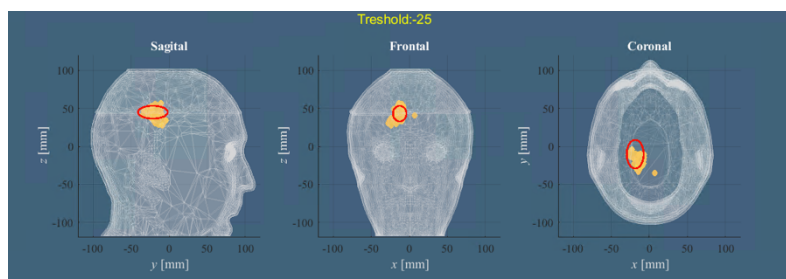


Figure 52. Three main planes views

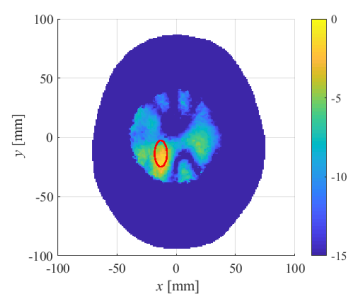


Figure 53. Energy map

### CASE 3

- target lateral central, frontal central, top central, depth lower
- time passed 61 minutes



Figure 54. Experimental set-up

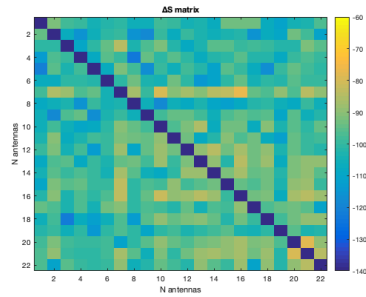


Figure 55.  $\Delta S$  matrix

### RECONSTRUCTION

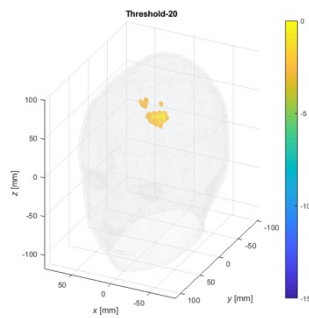


Figure 56. 3-D rendering

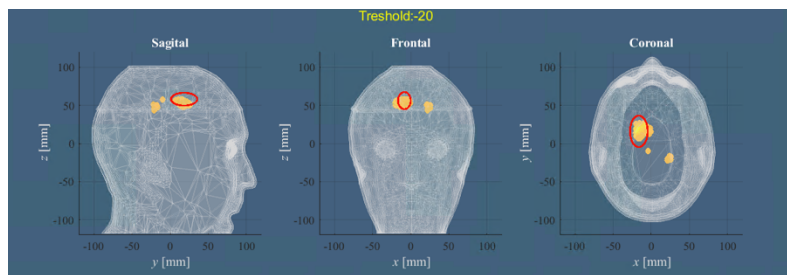


Figure 57. Three main planes views

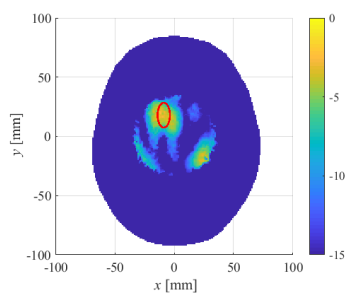


Figure 58. Energy map

The images obtained show the capability of the device to image even this new target similar to blood, although some inaccuracies in catching perfectly the position of the target and more noise in the images.

The shape of the reconstructed stroke is less regular than the one obtained with the sphere, but this is due to the irregular conformation of the balloon, which also gives more problems in managing it inside the brain liquid: the balloon, in fact, tends to move a bit once inserted in the phantom and to arrange obliquely (as can be seen especially in case1).

Moreover, using a different and precisely a more distant in time empty-measurement as a reference respect to which differentiate the target-measurements, the balloon is imaged the same showing already quite a stability in the system.

This is a basic model of stroke-target, but easier and faster to realize, however, in few days it begins to deflate so it does not last in time.

For this, the next step is to create a more controllable and stable model to simulate the hemorrhagic stroke.

## 4.3 Cylindrical case with blood

The last adopted target represents a more refined model of a stroke with a defined geometry.

It is realized using a small toy container in a very famous egg-shaped product (easily available in a supermarket), that is the plastic case inside the egg, whose shape can be approximate to a cylinder nearly 2.4 cm large, 4.5 cm long, with a radius of 1.6 cm and whose volume is almost 36 cm<sup>3</sup>.



*Figure 59. Cylindrical case*

The case is filled with the same blood liquid used for the latex balloon in this way: firstly, two very small holes are done on the top, then the liquid is injected inside through one of them with a syringe, while the other hole is useful to let the air out. Once filled the case, the holes are closed with a high strength glue and the target is wrapped with a piece of a latex glove to assure that the liquid does not come out. Two sticks are then attached to the cylindrical case at the extremities of its axe and at the end other wooden sticks are bounded to the vertical ones, so that it is possible to insert the target inside the phantom and to lean it in a sufficient stable way on its upper cavity.

The final target is reported in the figure 60.



*Figure 60. "Kinder egg" target*

The target so made is almost 20 cm long, but during the measurements some pieces of sponge are used so that the target can be placed at different depth and not only in different position; in particular, when the target is put higher it is closer to the eyes of the phantom, while when it placed lower it is closer to the top of the head.

In all the cases, the target is inserted with its vertical orientation, that is with its axe perpendicular to the eyes phantom.

The major number of measurements during the experimental assessment are acquired with this type of target and their reconstructions are always elaborated using a threshold range of -20 dB to -30 dB.

The image results are presented.

## CASE 1

- target position: lateral central, frontal central, top central slightly forward
- time passed 1 hour and 13 minutes

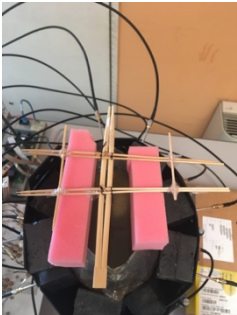


Figure 61. Experimental set-up

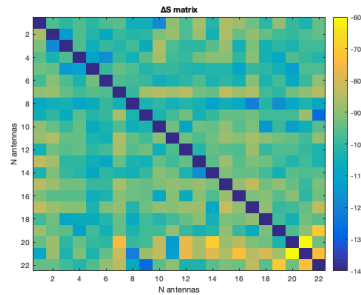


Figure 62.  $\Delta S$  matrix

## RECONSTRUCTION

The red symbol indicates the expected position of the target and it is an approximative estimate of its shape and dimensions

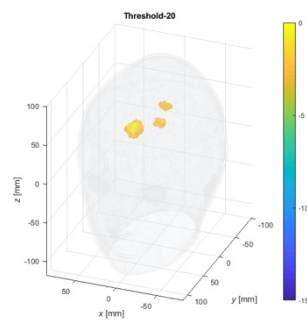


Figure 63. 3-D rendering

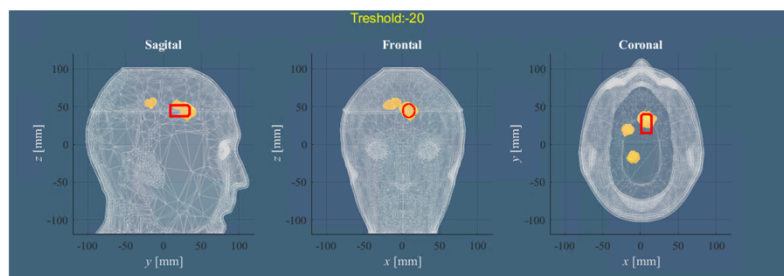


Figure 64. Three main planes views

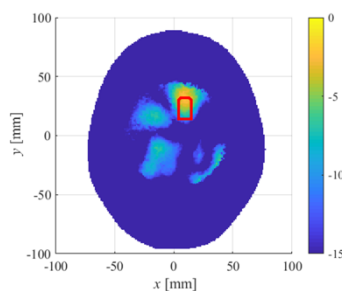


Figure 65. Energy map

## CASE 2

- target position: lateral central, frontal central, top central, closer to the eyes

- time passed 5 hours and 13 minutes



Figure 66. Experimental set-up

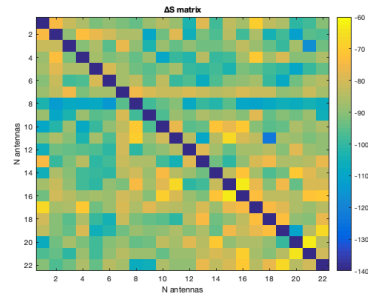


Figure 67.  $\Delta S$  matrix

## RECONSTRUCTION

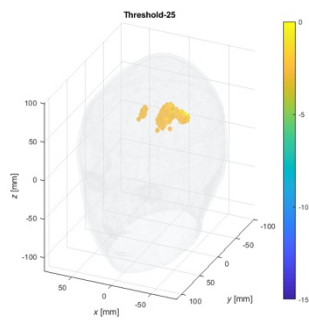


Figure 68. 3-D rendering

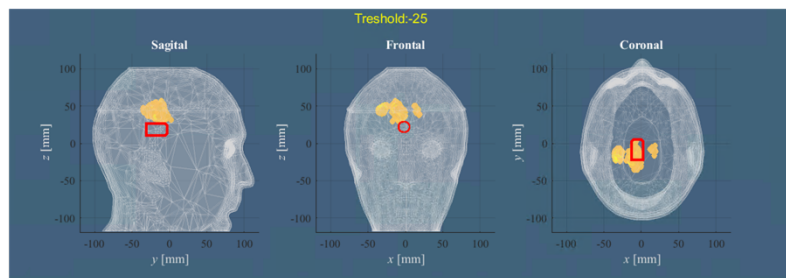


Figure 69. Three main planes views

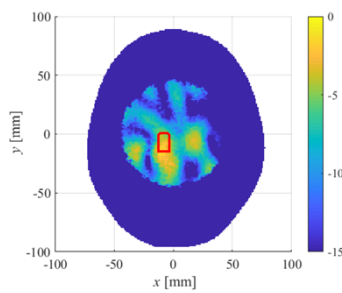


Figure 70. Energy map

### CASE 3

- target position: lateral central, frontal central, top central slightly to the left, closer to the top of the head

- time passed 2 hours



Figure 71. Experimental set-up

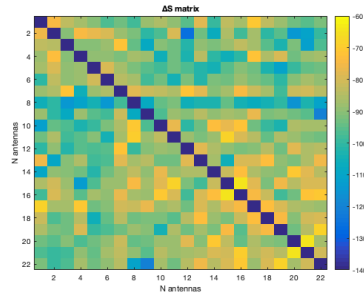


Figure 72.  $\Delta S$  matrix

### RECONSTRUCTION

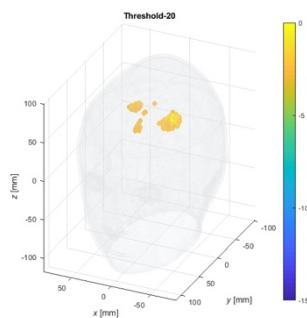


Figure 73. 3-D rendering

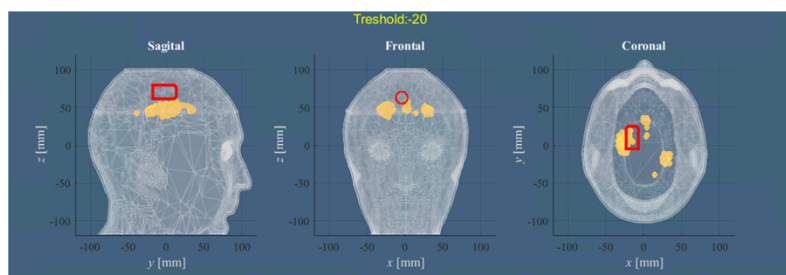


Figure 74. Three main planes views

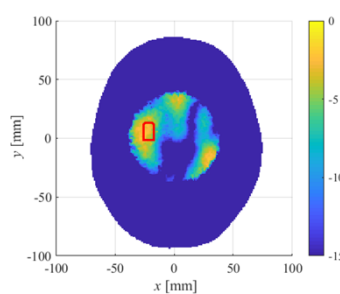


Figure 75. Energy map

It is already possible to notice from these initial cases that the device is still able to image even this new target.

The system, however, has difficulty in catching the right position especially as regard the height: even if the target is placed inside the phantom in a lower depth respect than a higher one, the image reconstructed reported the target at the same depth for both the cases, which is almost a central depth.

The images 75 a) and b), related to case 2 and case 3, show this comparison.

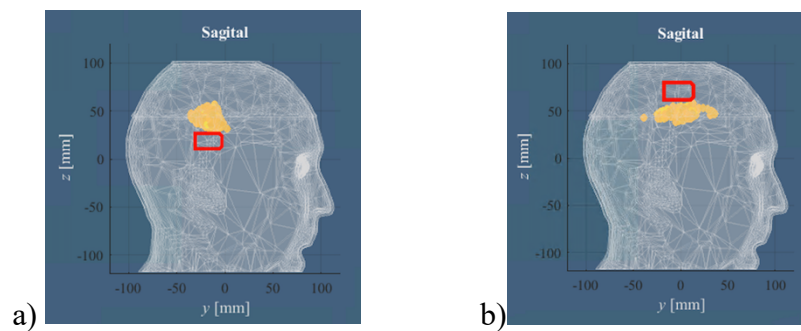


Figure 76. a) the target is expected to be seen almost at the same height of the eye, instead it is at central depth as in case b) where the target should be higher

The following cases, instead, are acquired placed the target at the same central depth but in different locations of the head phantom.

## CASE4

- target position: lateral central-back, frontal central, top central-back
- time passed 55 minutes



Figure 77. Experimental set-up

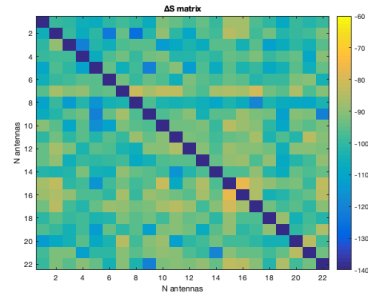


Figure 78.  $\Delta S$  matrix

## RECONSTRUCTION

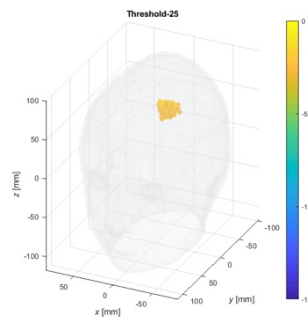


Figure 79. 3-D rendering

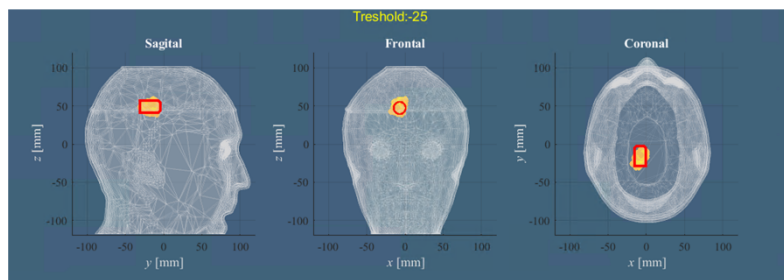


Figure 80. Three main planes views

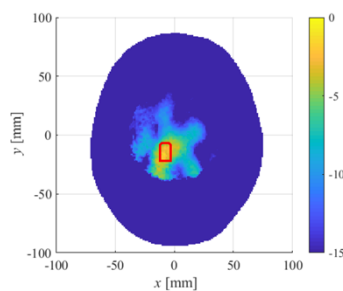


Figure 81. Energy map

## CASE5

- the same configuration of the case4 but using a different reference empty, which is more distant in time
- time passed 3 hours and 41 minutes

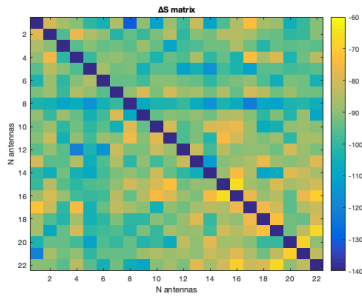


Figure 82.  $\Delta S$  matrix

## RECONSTRUCTION

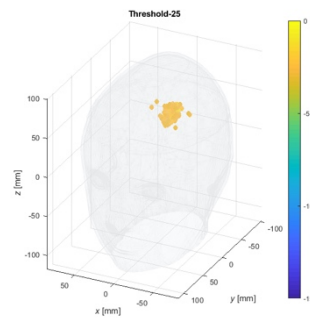


Figure 83. 3-D rendering



Figure 84. Three main planes views

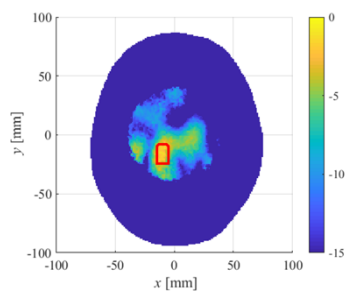


Figure 85. Energy map

These two cases confirm what it is already seen with the previous target: the prototype can reconstruct a correct image even taking a reference empty more distant in time respect to the measurement with the target.

Hence, exploiting different empties for the same target-measurement does not represent a limit for the system, which shows a quite good stability in the measurements during the time.

### CASE6

- target position: lateral central, frontal central-left, top central-left
- time passed 54 minutes



Figure 86. Experimental set-up

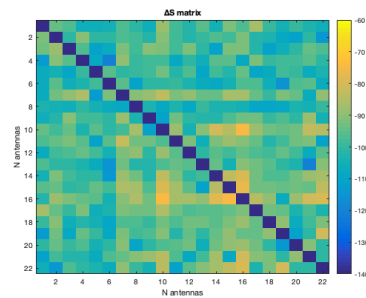


Figure 87.  $\Delta S$  matrix

# RECONSTRUCTION

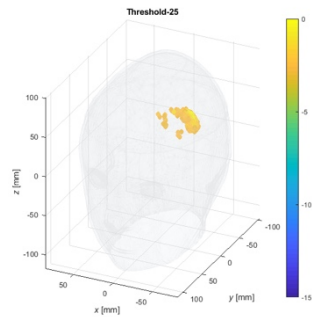


Figure 88. 3-D rendering

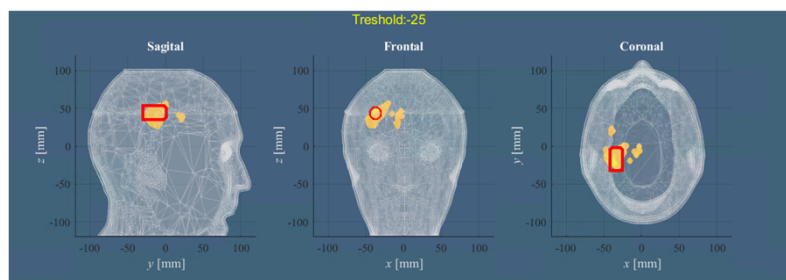


Figure 89. Three main planes views

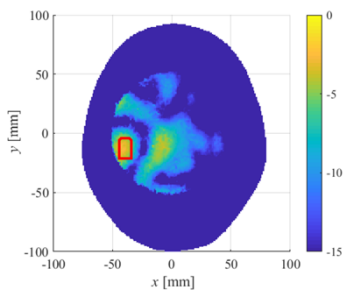


Figure 90. Energy map

## CASE7

- target position: lateral central-forward, frontal central, top central-forward
- time passed 3 hours and 8 minutes



Figure 91. Experimental set-up

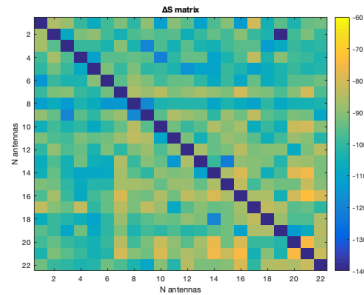


Figure 92.  $\Delta S$  matrix

## RECONSTRUCTION

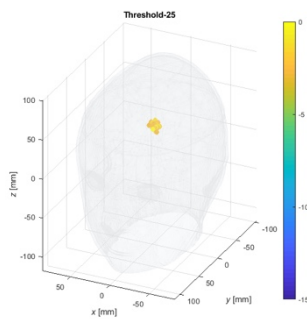


Figure 93. 3-D rendering

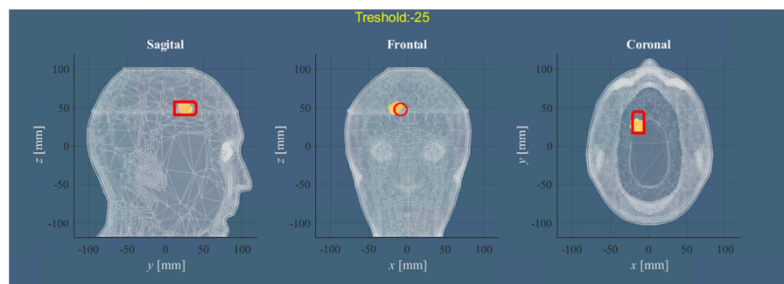


Figure 94. Three main planes views

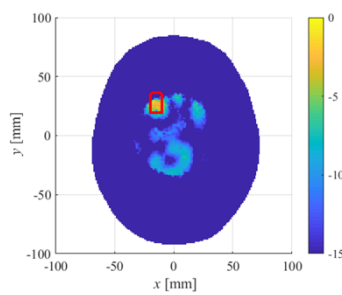


Figure 95. Energy map

Even if with inaccuracies in reproducing always the proper right shape or position of the target, as regards the reconstruction of the locations of the target in the head, the device is able to detect them more than detecting the different height positions; the yellow circle reconstructed in the images follows the position of the target in the experimental set-up, as visible in the comparison in Figure 96:

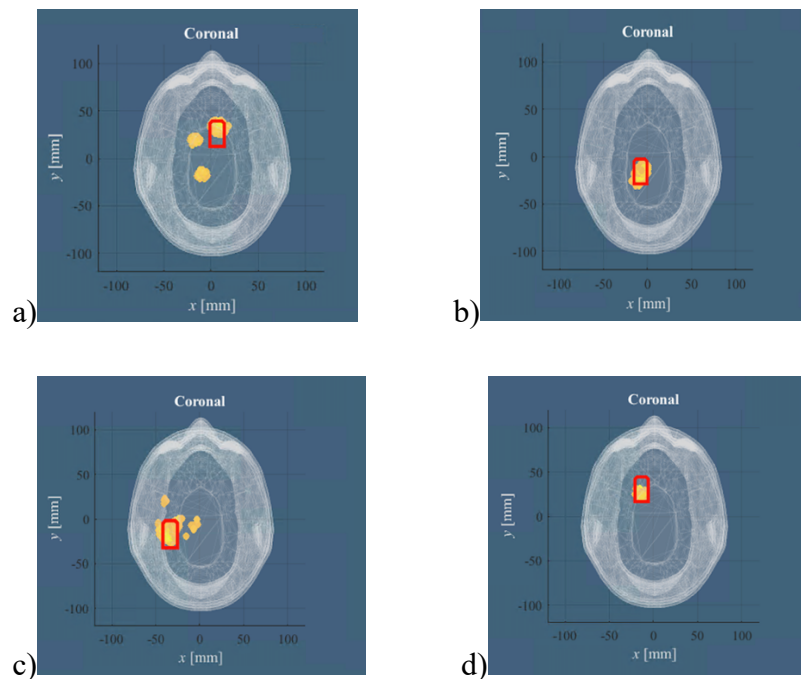


Figure 96. Different positions of the target reconstructed in the images: a) central slightly forward, b) back, c) at left, d) forward

Moreover, this new model of a stroke is easier to manage than the balloon, because it does not undergo great displacements when inserted in the brain liquid and it also lasts in time, since it does not deflate.

Its more regular shape, in addition, is suitable to be implemented in the simulation software to foresee the expected result of the measurement.

As said, what emerges from all the measurements made and the results obtained is that the device is capable of imaging the target and reconstructing it, in different experimental conditions; the system has, however, limitations particularly in the spatial resolution and in the sensitivity to perturbations.

To better analyze the behaviour of the system and to try to improve the quality of the measurements and so of the images, calibration procedures are investigated.

## 4.4 Calibration Procedures

### 4.4.1 External channels

As anticipated, the reconstructed images are affected by inaccuracies, which can be due to perturbations in the system, like temperature or measurement noise.

In preliminary studies, in fact, it is verified the effect of the temperature or in general of the variation of the conditions in the measurements room; three sets of measurements are acquired in three different weekends and they include consecutive measures lasting a total of almost two days for each set.

In particular the measures are taken removing the antennas 8 and 10 and connecting the two ports of the Switching matrix with a cable; in this way, the signals of the couples of antennas (8,10) and (10,8), which are nearly the same since the scattering matrix is symmetrical, should be constant and they do not depend on the object in the phantom.

These two signals are analyzed for each set, which present different measures configurations:

- set1 with empty head phantom (that is without the brain liquid) and without the VNA calibration
- set2 with empty head phantom but with the calibrated VNA
- set3 with the calibrated VNA and the phantom filled with brain liquid.

The behaviour in time of the two signals is shown in the figure 97.

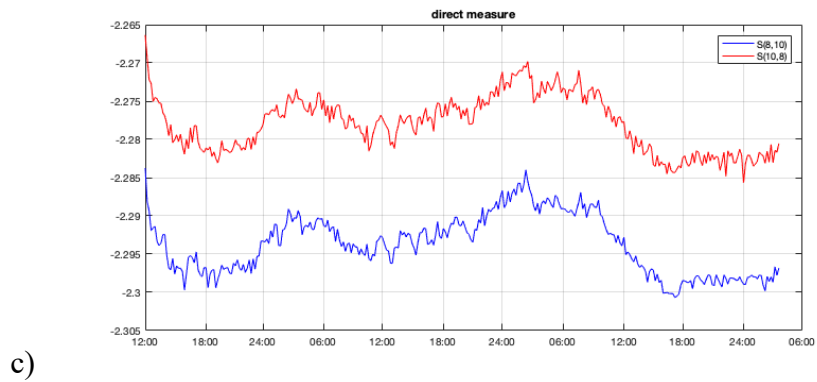
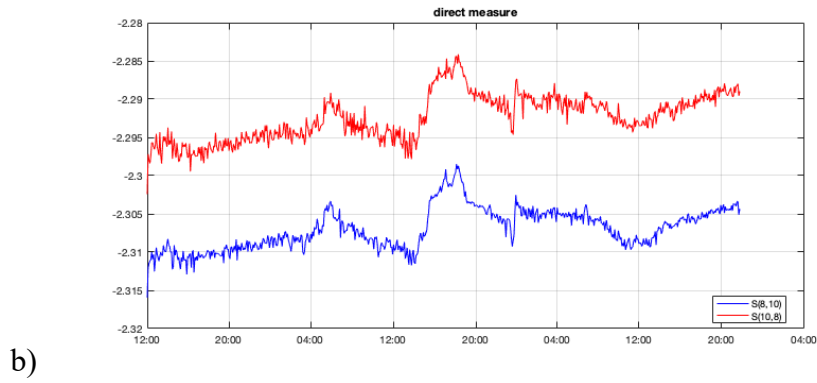
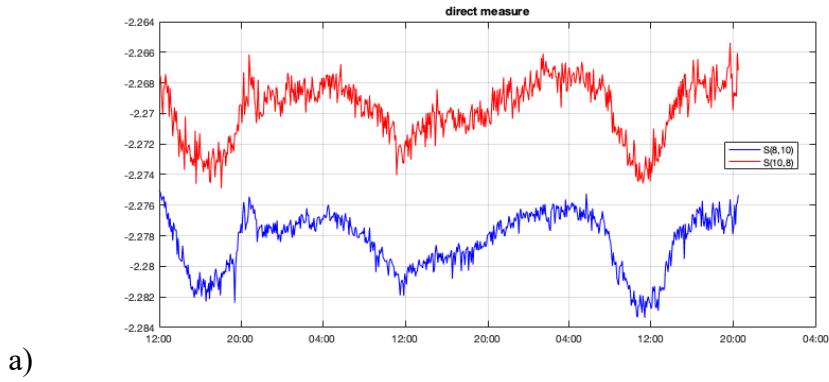


Figure 97. Signals in time related to antennas couples (8,10) and (10,8): a) set1, b) set2, c) set3

It can be seen that the signals of the cable are similar in each of three set and they are not exactly constant, but they show a variation during the time; in particular the trend of the signals is almost the same in the three measure configurations, representing a sort of “up and down”.

Starting from these considerations on the analyzed signals, which prove a variation in external environment during the measurements, a reference channel is realized.

As already said, two of the 24 antennas used for the acquisition are removed from the head phantom and put external to it; the signals related to the antennas 8 and 10, in this way, do not depend on the target and they should not change during the measurements.

The graphic in Figure 97 shows the signal in time correspondent to the couple of antennas (8,10), during the acquisition of a set of measurements in an afternoon:

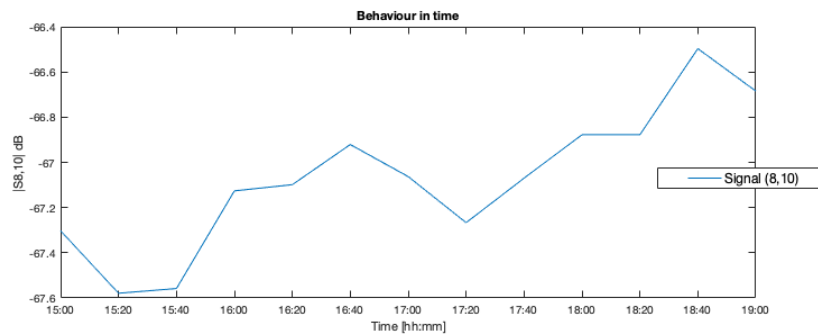


Figure 98. Couple (8,10) signals

Looking at the amplitude of the signal, it oscillates from a minimum of -67.5 dB and a maximum of -66.6 dB; the small variations, which are the same present, as seen previously, are not due to the target, but to some disturbances in the measurement room.

It can be caused by factors such as the temperature in the room, measurement noise, but also an approach of someone too near the system, whose interaction can perturb the scenario.

The signal derived from the two external antennas is, hence, taken as a reference.

## 4.4.2 Calibration with External Channel

The external channel related to the signal derived from the removed antennas 8 and 10, as explained, is considered as a reference signal so it is used to investigate a calibration procedure, in order to try to correct the measurements, extrapolating a correction factor to improve the quality of the reconstructed images.

This correction factor is obtained after derivation steps, which lead to the final equation, applicable to the  $\Delta S$  before giving it in input to the image algorithm, that is:

$$\Delta S = S^{empty}(t1) - (S^{ref}(t1) / S^{ref}(t2)) * S^{target}(t2) \quad (11)$$

where  $S^{empty}$  and  $S^{target}$  are the acquired Scattering matrices, related to the empty measurement and to the measurement with the target at time instants  $t1$  and  $t2$  respectively.

Preliminary test have been done using this calibration procedure, but they have not brought satisfactory results; other technical tests have been tried, such as a calibration with a numerical model, but they have not produce better results, for this, the images presented in the previous paragraphs are obtained without calibration and they still are the final results of the measurements proposed analysis.

The two antennas, however, are left outside the phantom, since they can be used for other investigations and they can constitute a further prof of what is going in the system during the measurements.

# 5 Further Analysis

## 5.1 Ictus Monitoring

One of the potentials of MWI technology is the possibility to do monitoring so to control the evolution of the stroke during the time.

Other measurements are performed to try to simulate a stroke monitoring, in order to understand if the device is able to detect changes in the stroke, which can be a growth or a shift of the hemorrhagic mass in the brain.

A first possible experimental set-up is tested in this thesis, as a first simple case to realize stroke monitoring, which consists in acquiring two consecutive measurements with the same target (that is the already assessed cylindrical case-target), respect to the same reference empty, but rotating it from a vertical position to a horizontal one, that is shifting the target clockwise thanks to the sticks.

In particular, firstly the target is inserted according to its vertical orientation inside the phantom, then it is rotated, arranging it horizontally; the two measurements are so reconstructed.

## VERTICAL CASE

- target lateral central, frontal central a bit right, top central a bit right
- time passed 1 hour and 34 minutes



Figure 99. Experimental set-up

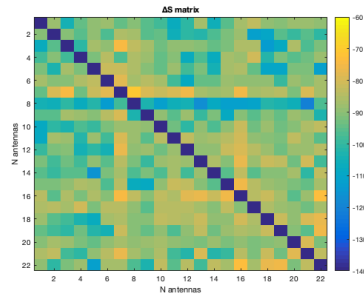


Figure 100.  $\Delta S$  matrix

## RECONSTRUCTION

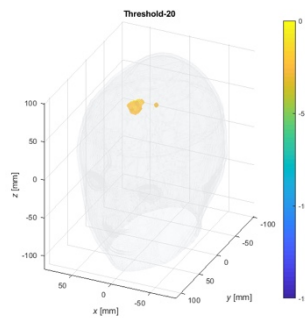


Figure 101. 3-D rendering

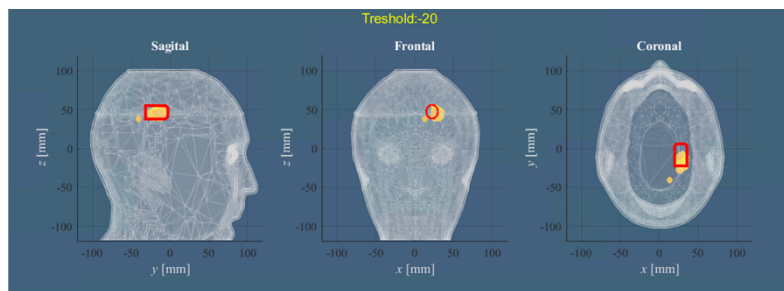


Figure 102. Three main planes views

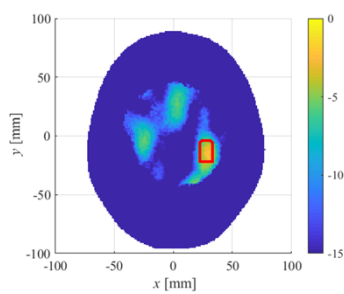


Figure 103. Energy map

## HORIZONTAL CASE

- target shifted clockwise
- time passed 1 hour and 54 minutes

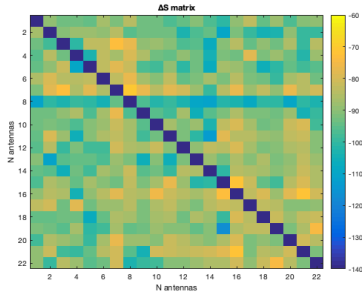


Figure 104.  $\Delta S$  matrix

## RECONSTRUCTION

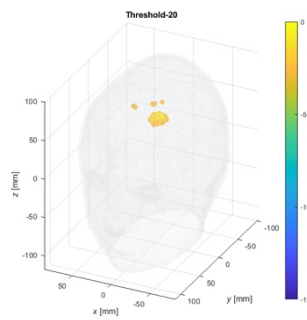


Figure 105. 3-D rendering

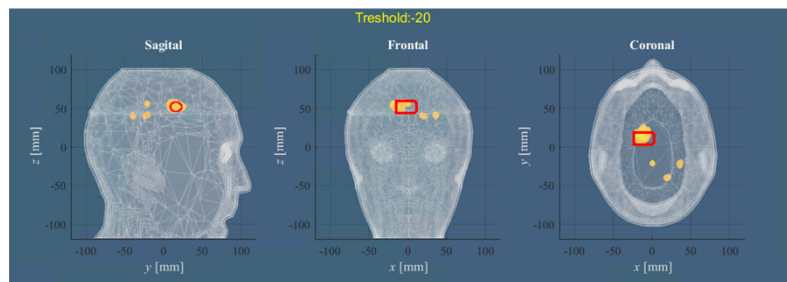


Figure 106. Three main planes views

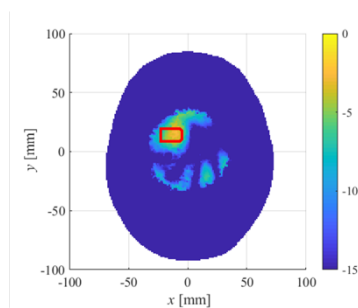


Figure 107. Energy map

The target is seen in different positions according to its different orientation in the experimental set-up; the difference between the two measurements with the two target conditions is also reconstructed.

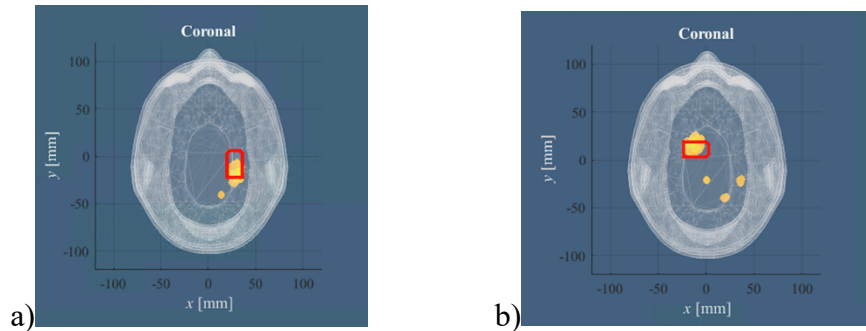


Figure 108. Comparison: a) vertical orientation, b) horizontal orientation

## DIFFERENCE CASE

- time passed 37 minutes

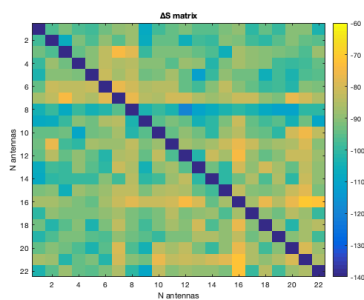


Figure 109.  $\Delta S$  matrix

## RECONSTRUCTION

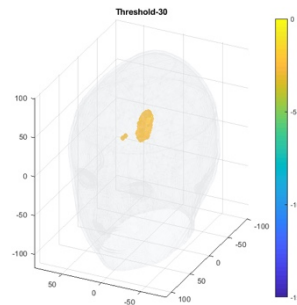


Figure 110. 3-D rendering

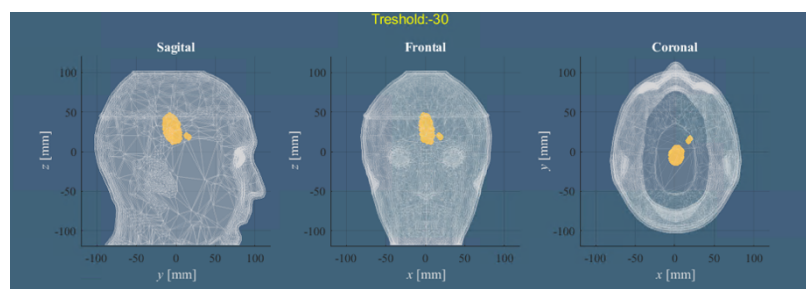


Figure 111. Three main planes views

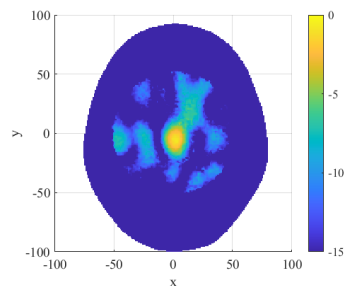


Figure 112. Energy map

The device detects the difference between the two the target positions, which is only a rotation of the same target around the surrounding area, occupied by the target itself.

It is an initial prof and it is under development, but it represents a possibility to mimic a stroke monitoring, hence, to image a variation in the brain affected area.

## 5.2 Multifrequency Analysis

As explained, each measurement is taken setting a range of frequencies and obtaining a Scattering matrix for each frequency; this is done in order to acquire more information, since having data not only for one frequency but even for 5 frequencies enables to understand more about the behaviour of the system.

For this, a multifrequency analysis is done with some initial tests, exploiting the measured scattering matrices related to two frequencies of the 5 present in the range; in particular the signals at 1.125 GHz and at 1.75 GHz are used.

A first method employed to get the image considering together the reconstruction of both the frequencies is the following: the contrast-function is computed as usual, using a differential Scattering matrix between the reference empty and the target, for each of the two frequencies with their respective TSVD operators, then the product point-by-point of the two contrast-vector is done.

This product is taken as reconstructed contrast to be plot in the same ways already used for the visualization of the previous images; the multifrequency analysis is so obtained multiplying the images collected by the single frequency analysis.

Three cases, already shown in the single frequency analysis (case2, case6, case4), are taken as example and are reported.

## CASE1

- target position: frontal central, lateral central, top central, closer to the eyes

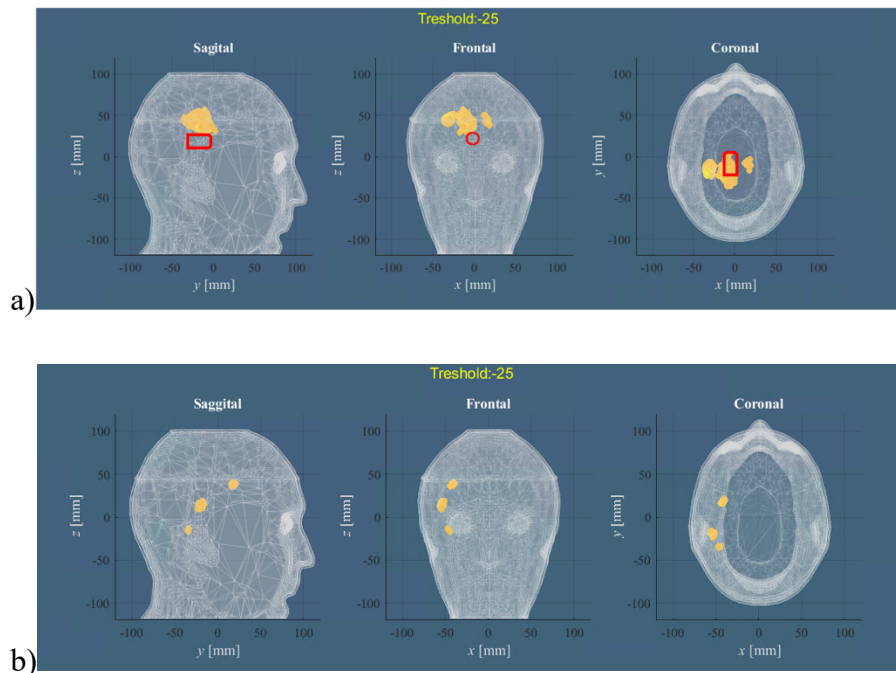


Figure 113. a) Single frequency, b) Multifrequency

## CASE2

- target position: frontal central, lateral central-left, top central-left

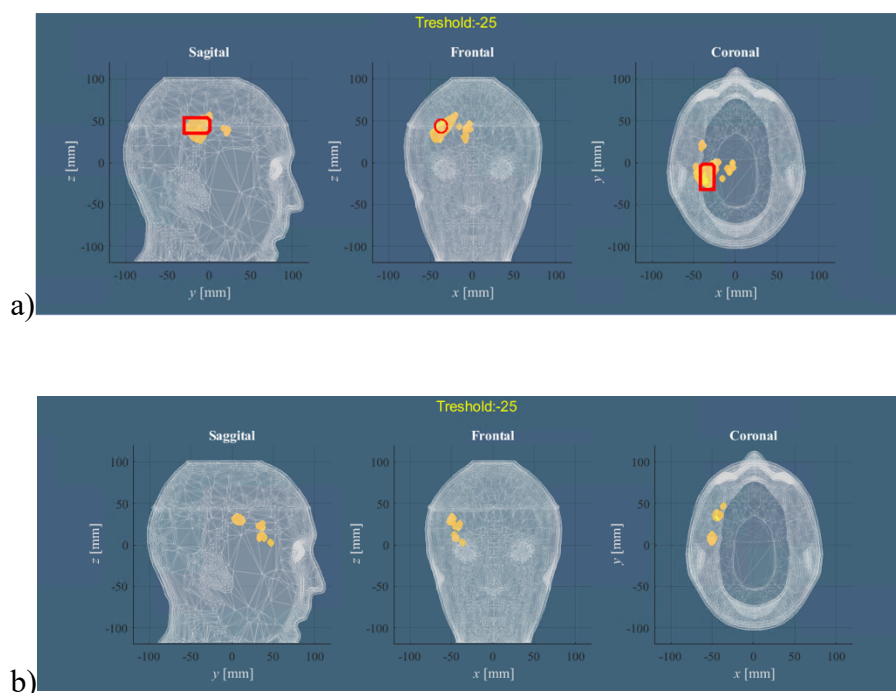


Figure 114. a) Single frequency, b) Multifrequency

### CASE3

- target frontal central, lateral central-back, top central-back

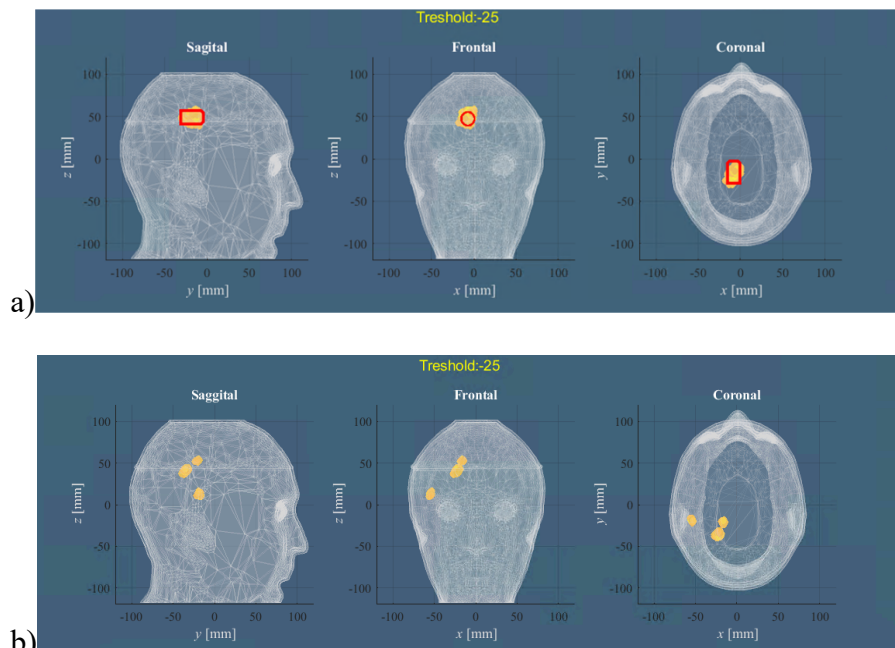


Figure 115. a) Single frequency, b) Multifrequency

As it appears from the results, the multifrequency images show a loss, since the target seems not to be evident anymore; this could be attributable to the fact that the frequency of 1.75 GHz begins to be too high with the risk not to assure a good penetration anymore.

This analysis, actually, can be done in other ways such as for example enlarging the TSVD operator or involving other frequencies, but is still under development and these tests are only an initial approach.

## 5.3 Check: “False Positive”

One last test is the verification of the so-called “false positive”, that is the reconstruction of the image obtained from two empty measurements, in order to understand the reliability of the MWI prototype.

The image derived from the difference of two empty Scattering matrices, in fact, should not reproduce anything so no yellow mass which stands for a target, since there is no object inside the phantom to be reconstructed.

This test, hence, is a further proof to demonstrate the operation of the device and some examples of reconstruction of “false positive” are presented below; they are two pairs of empties taken from the same set of measurements during a day and their images are normalized respect to the maximum value of the case with a target, precisely the case4 of the set with the cylindrical case-target.

### CASE1

- time passed between two empties acquisition 3 hour and 3 minutes

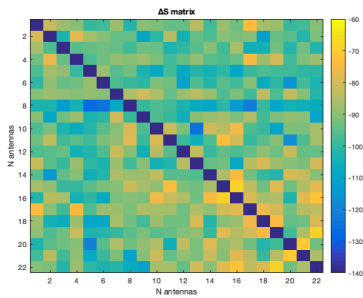


Figure 116.  $\Delta S$  matrix of two empties

### RECONSTRUCTION

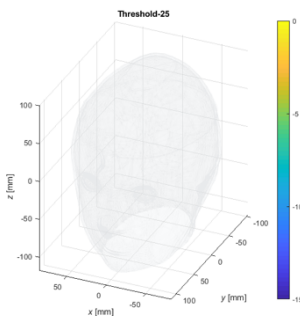


Figure 117. Three main planes views

## CASE2

- time passed between the two empties acquisitions 2 hour and 11 minutes

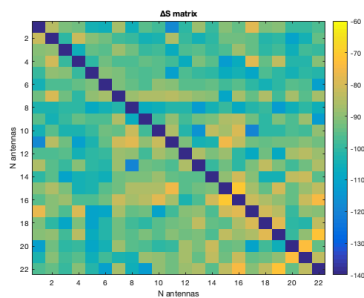


Figure 118.  $\Delta S$  matrix of two empties

## RECONSTRUCTION

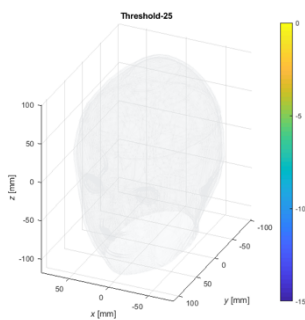


Figure 119. 3-D rendering

Both the two cases show no detection, since there is no target in the phantom and the reconstructions result empty.

Calculating the maximum value of their contrast function, in fact, it is much lower than the maximum of the case with the target (respect to which the empty cases are normalized); for both cases it is around -170 dB and for this reason, it cannot be represented in the range of 15 dB to 0 dB.

Moreover, also through the following energy maps, it is possible to see that the reconstructions of the empties show intensity values lower than the ones in general

present in the cases with a target; the maximum value in the images with the empties, in fact, is much lower than 0 dB, as it happens when there is the target.

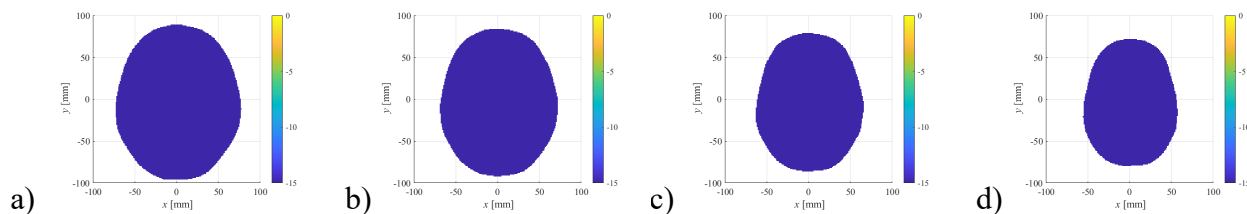


Figure 120. Horizontal cross-section at various level, differentiating measurements with the same scenario (two empties): case1 a)  $z=40$  mm, b)  $z=50$  mm, c)  $z=60$  mm; case2 d)  $z=70$  mm

## 6 Discussion

The aim of the presented experimental campaign, with its data elaboration, is to validate the capability of the MWI prototype to image a possible stroke inside the human brain, in order to provide clinicians with a further support in addition to the existing diagnostic neuroimaging techniques, such as MRI and CT.

The reported results prove that the device is able to detect an object inside the phantom, both a small target, as a plastic ball of a nearly 1.25 cm of radius, and targets of bigger dimensions, which simulate a hemorrhagic stroke; precisely, the plastic sphere is reconstructed with greater accuracy as regard its shape, because actually it is more defined, while the other two targets tested are reproduced not always with their proper shape, since it is less regular so more difficult to be identified exactly, and this happens especially in the measurements with the balloon, whose images are in fact noisier; this is also why a more realistic target is then employed to mimic the affected brain region.

The MWI system, moreover, can recognize the different positions in which the target is placed during the measurements, reconstructing the object in different locations according to their change in the experimental set-up, although the real position is not always caught perfectly; sometimes there is a difference between the reproduced position in the image and the estimate of the one expected.

This difference is also due to the fact that the target, when inserted in the brain liquid, tends to move slightly and not to stay in the correct position it is supposed to be inserted; however, as already said during the report of the results, although imperfections in matching the real position, the device can notice and reconstruct different locations.

In addition, the prototype proves to be robust respect to the false positive, as assessed through the reconstructions of differential measurements without the target and hence with the same scenario; it also demonstrates quite a stability in the results, when

repeating the measurements and when differentiating the acquisition with the target with different empty-measurements at different time intervals.

The current limits of the device, however, resides in the spatial resolution, which is only on the order of a centimeter, and in the sensitivity to various factors, such as temperature, measurement noise, the presence of air bubbles in the brain liquid when inserting the target or even the presence of someone too near to the system; all these conditions may contribute to perturb the acquisition and to the provide noisier images, where there is not only a clear mass, representing the target, but also some other spots.

In this regard, the calibration procedure tested to attempt to correct the errors, especially the one with the two external antennas, is not sufficient to compensate these inaccuracies and the images obtained are valid without the calibration; it is worth keeping the reference channel, since it constitutes the same a further information about the behaviour of the system and it can be analyzed to see if something happens during the measurements.

# 7 Conclusion and Future Perspectives

In the thesis, a low-complexity Microwave Imaging prototype, aimed to detecting brain stroke, has been presented and a series of experimental measurements and respective image reconstructions has been carried out, in order to validate the potential of the proposed device to imaging possible anomalies in the head.

This has been assessed through the results derived from a detailed elaboration of the experimental acquisitions with different models of stroke-target, which confirm the possibility of realizing new diagnostic images complementary to the one already consolidated [32].

MWI technology, in fact, enables a safety and practical scan of the brain particularly suitable to evaluate the state of a stroke after its onset and to do a continuous monitoring of the pathology.

Since the device is still a prototype, there are several tests which can be performed to improve this model and prove its working, both experimentally and in elaboration procedures.

Firstly, the multifrequency analysis and an experimental simulation of stroke monitoring have been tested as initial trials, but they are still under development.

Then, possible future steps consist in the realization of a smaller target, even using the cylindrical case-target but with reduced dimensions, to apply in the measurements in order to see the capabilities of the device to image and to properly reconstruct a smaller object acting as stroke; another development, moreover, is the simulation of an ischemic stroke, which can be done using always the same type of target of the hemorrhagic one, but filled with a liquid with a slightly different composition than the one acting as a hemorrhagic stroke, so that it can simulate a clot instead of a hemorrhage.

To conclude, the proposed system is still a prototype and improvements are required to refine the device so as to achieve the final goal of creating a wearable 3-D MWI

helmet, that is a portable device, which permits a timely scanning even right in ambulance, repeated examinations and monitoring also bedside.

It is till now a satisfying starting point for a new imaging technology, which really can save the life of many people.

# Bibliography

[1] “National Heart,Lung and Blood Institute”, available at

<https://www.nhlbi.nih.gov>

[2] “American Stroke Association”, available at <https://www.stroke.org/en/about-stroke>

[3] Benjamin, E.J.; Muntner, P.; Bittencourt, M.S., “Heart Disease and Stroke Statistics—2019 Update: A Report from the American Heart Association.”

Circulation 2019, 139, e56–e528.

[4] C. Johnson et al.,“Global, regional, and national burden of stroke, 1990–2016: a systematic analysis for the Global Burden of Disease Study 2016”, The Lancet Neurology, vol. 18, no. 5, pp. 439–458, 2019.

[5] Valery L. Feigin, Bo Norrving, George A. Mensah, “Global Burden of Stroke”, Circulation Research Compendium on Stroke, 2017;120:439-448

[6] Nour, Liebeskind, “Brain Imaging in Stroke: Insight Beyond Diagnosis”, The American Society of Experimental Neurotherapeutics, Neurotherapeutics (2011) 8:330–339

[7] F. Molinari, Slides of the course “Bioimmagini-Tomografia Computerizzata”, Politecnico di Torino

[8] J. M. Wardlaw, “Radiology of Stroke”, J Neural Neurosurg Psychiatry 2001, 70 (suppl I):i7–i11

[9] F. Molinari, Slides of the course “Bioimmagini-Fondamenti Risonanza magnetica”, Politecnico di Torino

- [10] Philip MRI
- [11] K. P. Lho, S. Ramdass, L. Howard, S. Dahiya, “Association between Thrombophilia and Ischemic Stroke: when is work-up for hypercoagulable state indicated?”, *Clinical Case Report and Review*, Volume 2(4): 380-382
- [12] R. Scapaticci, M. Bjelogreis, J. A. Tobon Vasquez, F. Vipiana, M. Mattes, L. Crocco, “Microwave Technology: Physical Foundations, Potential and Limitations”
- [13] P. Kosmas, L. Crocco, “Microwave Imaging for Medical Diagnostic: from theory to implementation”, *Eucap Workshop*
- [14] European School of Antennas, Short course “Antenna Imaging Techniques”, *Universitat Politecnica de Catalunya 2013*
- [15] A. La Gioia, E. Porter, I. Melunka, A. Shahazad, S. Salahuddin, M. Jones, M. O’Halloran, “Open ended coaxial probe technique for Dielectric Measurements of Biological Tissues: Challenges and Common Practice”, *Diagnostics*, June 2018
- [16] C. Gabriel, S. Gabriel, E. Corthou, “The dielectric properties of biological tissues: I. Literature Survey”, *King’s College London, UK, 1996*
- [17] A. Fhager, S. Candefjord, M. Elam, M. Person, “Microwave Diagnostic Ahead”
- [18] J.A. Tobon Vasquez, Slides of course “Microwave Sensing and Imaging for Innovative Applications in Health and Food Industry”, *Politecnico di Torino 2020*
- [19] R. Chandra, H. Zhou, I. Balasingham, R. Narayanam, “On the opportunities and challenges in Microwave Medical Sensing and Imaging”, *IEEE Transactions on Biomedical Engineering*

- [20] Stefan Blügel, “Scattering Theory: Born Series”, Scattering Methods for Condensed Matter Research: Towards Novel Applications at Future Sources
- [21] R. Scapaticci, M. Bjelogrljic, J. A. Tobon Vasquez, F. Vipiana, M. Mattes, L. Crocco, “Microwave Technology for Brain Imaging and Monitoring: Physical Foundations, Potential and Limitations”
- [22] R.Scapaticci, L. Di Donato, I. Catapano, L. Crocco, “A Feasibility study on Microwave Imaging for Brain Stroke Monitoring”, Progress in electromagnetic research, vol. 40, 305-324, 2012
- [23] J. A. Tobon Vasquez, R.Scapaticci. G. Turvani, G. Bellizzi, N. Joachinowicz, B. Duchene, E. Tedeschi, M. R. Casu, L. Crocco, F. Vipiana, “Design and Experimental Assessment of a 2-D Microwave Imaging System for Brain Stroke”
- [24] J. A. Tobon Vasquez, Slides of the course “Microwave Sensing and Imaging for Innovative Applications in Health and Food Industry”, Politecnico di Torino 2020
- [25] J. A. Tobon Vasquez, R. Scapaticci, G. Turvani, G. Bellizzi, D. O. Rodriguez Duarte, N. Joachinowicz, B. Duchene, E. Tedeschi, M. R. Casu, L. Crocco, F. Vipiana, “ A Prototype Microwave System for 3-D Brain Stroke Imaging”, Sensors
- [26] <https://www.mdpi.com/2075-4418/8/4/85/pdf/1>
- [27] <https://www.keysight.com/it/en/home.html>.
- [28] R. Scapaticci, O. M. Bucci, I. Catapano, L. Crocco, “Differential Microwave Imaging for Brain Stroke Followup”, Hindawi Publishing Corporation International Journal of Antennas and Propagation Volume 2014, Article ID 312528, 11 pages

- [29] D. O. Rodriguez Duarte, J. A. Tobon Vasquez, R. Scapatucci, L. Crocco, F. Vipiana, “Assessing a Microwave Imaging for Brain Stroke Monitoring via High Fidelity Numerical Modeling”, *IEEE Journal of Electromagnetics, Rf and Microwave in Medicine and Biology*
- [30] F. Vipiana, Calibration Notes, Politecnico di Torino
- [31] C. Gilmore, P. Moyobi, A. Zakaria, M. Ostradrahimi, C. Kaye, S. Noghianian, L. Shafai, S. Pistorius, J. LoVetri, “A Wideband Microwave Tomography System with a Novel Frequency Selection Procedure”, *IEEE Transactions on Biomedical Engineering*
- [32] S. Semenov, “Microwave tomography: review of the progress towards clinical applications”, *Philosophical Transaction A*, 2009 Aug 13; 367(1900): 3021–3042.

# Thanks

At the di end of my thesis, I really would like to thank Professor Francesca Vipiana and Professor Jorge Alberto Tobon Vasquez for guiding me along this route from start to finish and for giving me the opportunity to take part of a stimulating innovating project, which has contributed to expand my knowledge and to experience something practical in a new laboratory, even at a time when working remotely seemed to be the only job possible.

I sincerely thank Engineering David Orlando Rodriguez-Duarte for the precious support and the advices given to me to perform in the best way my work, making the collaboration not only fruitful but also enjoyable.

I thank in general all the people I have know in the LACE, for the familiar atmosphere created inside the laboratory.

So thank you all for helping me to close my course of studies in a more satisfactory way.